Thermal and exhumation histories of the northern subalpine chains (Bauges and Bornes – France): evidences from forward thermal modeling coupling clay mineral diagenesis, organic maturity and carbonate clumped isotope (Δ_{47}) data.

Xavier Mangenot[1,2,3], Jean-Francois Deconinck[1], Magali Bonifacie[2], Virgile Rouchon[3], Pierre Yves Collin[1], Didier Quesne[1], Marta Gasparrini[3], Jean-Pierre Sizun[4]

[1] Biogéosciences, UMR 6282 CNRS, Université Bourgogne Franche-Comté, 6 Boulevard Gabriel, 21000 Dijon, France

[2] Institut de Physique du Globe de Paris, Sorbonne Paris Cité, Université Paris Diderot, UMR 7154 CNRS, 75005 Paris, France.

[3]IFP Energies nouvelles, 1-4 avenue de Bois-Préau, 92852 Rueil-Malmaison, France

[4] Chrono-environnement, UMR 6249 CNRS, Université Bourgogne Franche-Comté, 16 route de Gray, 25030 Besançon, France

ABSTRACT

Assessing the thermal evolution of sedimentary basins over time is a major aspect of modern integrated basin analysis. While the behavior of clay minerals and organic matter with increasing burial is well documented in different geological and thermal settings, these methods are often limited by the temperature ranges over which they can be precisely applied and by the available material. Here, we explore the emergent Δ_{47} clumped isotope thermometry (based on the diffusional redistribution of heavy carbon and oxygen isotopes in the carbonate lattice at elevated temperatures) to refine time-temperature paths of carbonate rocks during their burial evolution. This study provides a reconstruction of the thermal and exhumation history of the Upper Cretaceous thrust belt series in the western subalpine massifs (Bauges and Bornes, French Alps) by a new approach combining available data from three independent geothermometers. The investigated area presents two zones affected by contrasting thermal histories. The most external zone has undergone a relatively mild thermal history (T < 70°C) and does not record any significant clay mineral diagenetic transformation. By contrast, the internal zone has experienced tectonic burial (prealpine nappes) in response to thrusting, resulting in overheating (T > 160-180°C) that induced widespread clay mineral diagenetic transformations (progressive illitization from R0 to R1 and R3 illite-smectite mixed-layers), organic matter maturation (oil window) and Δ_{47} thermal resetting with apparent equilibrium temperatures above 160°C. The three employed geothermal indicators conjointly reveal that the investigated Upper Cretaceous rocks have suffered a wide range of burial temperatures since their deposition, with a thermal maximum locally up to 160-180°C. High temperatures are associated with the tectonic emplacement of up to 4km of prealpine nappes in the northern part of the studied area.

Finally, a forward thermal modeling using the kinetic algorithms for Δ_{47}, vitrinite reflectance and clay mineral data, is attempted to precisely refine the time-temperature evolution of these rocks during burial and exhumation.

KEY-WORDS: subalpine massifs, Δ_{47} clumped isotope thermometry, Thermicity, Clay diagenesis, Kinetic models.

INTRODUCTION

Assessing the thermal evolution of sedimentary basins over time is a major goal of modern integrated basin analysis, especially in areas where major erosion occurred, such as the fold and thrust belts. This requires looking for past thermal conditions recorded by the modifications of minerals and organic matter. Among the numerous temperature dependent transformations occurring during burial and uplift, vitrinite reflectance and apatite fission track annealing are the most widely used for studying the evolution of low-temperature systems (ie., 60-100°C). At higher temperatures (i.e., 80-200°C), other kinetically-dependent indicators can be used to assess past thermal conditions, including the T_{max} parameter from kerogen Rock-Eval pyrolysis (Espitalié et al. 1985), the illite crystallinity index (otherwise named "Kubler index" ; Kubler & Jaboyedoff, 2000) and the decrease in smectite content in mixed-layered illite/smectite (I-S ; Inoue et al. 1987). In this context, coupling different methods together may provide a more reliable dataset to refine paleo-thermicity reconstructions, especially when each employed technique has its own kinetic dependence to the burial and time-temperature histories.

However, the kinetic response of clay mineral reactions, such as illitization of smectite, can vary significantly from that of vitrinite, mainly due to strong inhibiting effects of the Na^+, Ca^{2+} and Mg^{2+} release on the illitization (Roberson & Lahann, 1981; Howard & Roy, 1985). Lithology is an additional issue when correlating mineral and organic matter thermal indicators. Generally, limestones and sandstones are not suitable, largely because they do not contain sufficient clay. Moreover, these lithologies can either inhibit clay mineral reactions, through early cementation or promote reactions through pore fluid movement, which are not comparable with reaction conditions in pelitic rocks (Aldega et al. 2005; Honlet et al. 2017). In this study, we present results of a correlation between vitrinite reflectance and illite content in illite-smectite (I-S) mixed-layers in a clay-poor limestone unit, that we combine here for the first time with carbonate clumped isotopes thermometry (Δ_{47}).

The emergent carbonate clumped isotope Δ_{47} thermometry relies on an internal equilibrium within the carbonate lattice with rare, heavy isotopes (notably ^{13}C and ^{18}O) preferentially bonding to each other at low temperature. The abundance of $^{13}C^{18}O^{16}O_2$ groups in carbonate lattices relative to its random distribution depends on temperature (Schauble et al., 2006). This Δ_{47} dependence to temperature has been experimentally determined for several types of carbonates (e.g., Dennis and Schrag, 2010; Henkes et al., 2013; Kele et al., 2015; Bonifacie et al., 2017; Katz et al., 2017; Kelson et al., 2017) and can be applied to virtually any (Ca, Fe, Mg)CO_3 carbonate in the 0-350°C geologically-relevant temperature

range (Bonifacie et al., 2017). Over the last decade, the Δ_{47} thermometry has been mostly applied for paleoclimatic reconstructions of fossil carbonates, with more recent application to reconstruct mild diagenetic conditions (ie., below 100°C) as for example by reconstructing paleotemperatures and fluid chemistries associated with cements and fractures (e.g., Bristow et al., 2011; Huntington et al., 2011; Budd et al., 2013; Loyd et al., 2013; Mangenot et al., 2018 and 2017; Pagel et al., 2018), faults (Swanson et al., 2012; Bergman et al., 2013; Fay-Gomor et al., 2018), and concretions (Loyd et al., 2012; Dale et al., 2014) or identifying cryptic recrystallization of carbonate fossils (Bennett et al., 2018). However, when carbonates experience high temperatures, the initial abundance of $^{13}C^{18}O^{16}O_2$ groups (and thus the Δ_{47} value acquired at the time of precipitation) might change due to diffusional reordering of isotopes within the carbonate lattice. This process can happen on both the prograde and retrograde paths during a geological heating event (e.g., Passey and Henkes, 2012), and without any dissolution/recrystallization of the carbonate phase or imparting noticeable changes to bulk isotopic compositions ($\delta^{13}C$ and $\delta^{18}O$), elemental concentrations, or mineral textures. This has been first highlighted in metamorphic marbles that generally show apparent equilibrium temperatures of about ~150-200°C for calcites (Ghosh et al., 2006; Bonifacie et al., 2013) despite peak metamorphic temperatures far above 500°C. This apparent temperature for marbles is thought to represent the "blocking" temperature with respect to diffusional resetting of the carbonate clumped isotope thermometer – that is the temperature at which the isotopes stop exchanging by solid state diffusion during gradual cooling (e.g., Passey and Henkes, 2012; Bonifacie et al., 2013). Later studies allowed to determine that for calcites exposed to temperatures in excess of 75–100°C over hundreds of millions of years this process can affect the Δ_{47} composition such as it wholly or partially reflects the temperature experienced by the ambient rocks (Passey and Henkes 2012; Stolper and Eiler, 2015). Those experimental and theoretical studies also allowed to build a kinetic framework describing the rates of solid state reordering during heating and cooling. Overall, this phenomenon provides a way to use Δ_{47} as a geospeedometer and to reconstruct heating and cooling path conditions (e.g., Bristow et al., 2011; Passey and Henkes, 2012 ; Bonifacie et al., 2013 ; Henkes et al., 2014 ; Stolper and Eiler, 2015). Here, we exploit this kinetic behavior of Δ_{47} as an emerging archive of basin thermal histories, as recently done for thermal history evaluation of natural carbonates (Shenton et al. 2015 and Lawson et al., 2017). In this work, we couple for the first time this kinetic behavior of Δ_{47} clumped isotopes thermometry with clay mineralogy thermometry, and previously published vitrinite reflectance data, in order to refine the current knowledge on the burial and exhumation evolution of an Upper Cretaceous limestone unit cropping out in the subalpine chains of the western French Alps (Bauges and Bornes massifs).

GEOLOGICAL SETTING

The northern subalpine chains of France, is a fold-dominated thrust belt consisting of Mesozoic and Cenozoic sedimentary strata located between the Molasse foreland Basin to the northwest and the External Crystalline Massifs (ECM) to the southeast (e.g., Bellahsen et al., 2014, Fig. 1). The northern subalpine chains (Bauges and Bornes massifs) are structurally

beneath the Prealps (Chablais nappe), which were emplaced by the Helvetic thrust that has since been eroded, leaving Sulens and Annes klippes, as remnants of the Prealps nappes on the Bauges and Bornes massifs (Fig. 1). These thrust sheets are made of various Mesozoic and Cenozoic strata derived from the more internal domains of the Alps compared to the ECM. The maximal geographical extent and the thicknesses of these thrusting units are poorly defined because they were mainly eroded during Plio-Pleistocene times. Since the 1970's, several paleothermal proxies have been investigated to estimate the thermal, diagenetic and structural histories of these chains, and to attempt to predict the thickness of the tectonic belts emplaced onto the subalpine chains during the final stages of the alpine compression. The pioneering works of Kübler et al. (1974) and Sawatzki (1975) revealed an increasing low-grade metamorphism from the northern subalpine massifs in Haute-Savoie towards the Swiss Alps in the Northeast. Then, Deconinck & Debrabant (1985) highlighted important diagenetic transformations of clay mineral assemblages in Upper Cretaceous carbonate deposits ("sublithographic limestones"), expressed by a systematic increase of illite and chlorite at the expense of smectite in the more internal domain of the northern subalpine chains. They interpreted the mineralogical evolution as the expression of the tectonic overload (prealpine nappes) in the eastern part of the subalpine basin. Consistently, more recent data on vitrinite reflectance revealed an increase of organic matter thermal maturation in the northeastern part of the subalpine chains (Gorin & Monteil, 1990, Butler, 1991; Moss, 1992). Such a combination of independent thermal indicators indicates that the northeastern part of the chain suffered higher temperatures, due to the greater tectonic loads exerted onto the subalpine chains. Thermal data and modeling results suggest that the eastern Bornes and Bauges massifs have experienced a burial depth up to *5* km greater than their western areas (Moss, 1992). Butler (1991) estimated maximal temperatures induced by this tectonic load around 180°C in the eastern domain and 60-70°C in the western domain.

MATERIAL AND METHODS:

Field samples collection

This study focuses on a Late Cretaceous calcareous unit called the "sublithographic limestones" ranging in age from the Turonian to the Campanian (Villard, 1991). The major rock-forming constituents are micrite particles, calcareous ooze, and allochems fragments, including planktonic and benthonic foraminifera and calcispheres (coccolithes fragments). These limestones were chosen for the two following reasons: (1) the "sublithographic limestones" consist of a fine grained and homogeneous micritic formation containing small amounts of clay minerals (<5%), allowing for clay diagenesis and Δ_{47} composition to be measured conjointly on the same samples, and (2) it is a well exposed unit across the fold and thrust belt this allowing for collecting samples through a large range of low-grade metamorphism domains. The "sublithographic limestones" are generally well-exposed to the heart of the synclines of the Bauges and Bornes massifs. They superimpose condensed horizons of glauconite and phosphate bearing green sandstones of Aptian/Albian age (Delamette et al., 1997) and are unconformably overlain by Cenozoic deposits (Fig. 2). A total of 110 samples were collected from 18 sites (Fig. 1) for XRD analyses, from which 8

representative samples were targeted for petrophysical measurements and Δ_{47} thermometry analyses.

X-ray diffraction analyses

Clay mineral assemblages were identified by XRD on oriented mounts of non-calcareous clay sized particles (<2µm) following the procedure described by Moore & Reynolds (1997). The XRD apparatus is composed of a Bruker D4 Endeavor diffractometer with CuK_{α} radiations with a Lynx-eye detector, Ni filter, and under 40kV voltage and 25 mA intensity. Three preparations were analyzed for each sample: (1) a first after air-drying (AD), (2) a second after ethylene-glycol (EG) solvation and (3) a third after heating at 490°C for 2h. The goniometer scanned from 2.5° to 28.5° for each run. Identification and semi-quantitative estimates of clay minerals were made according to the position of the (001) basal reflection on the three XRD (AD, EG and heated). The quantification of smectite and illite layers (%S and % I respectively) in illite-smectite mixed-layers minerals (I-S) is estimated on oriented clay sized particles following two different methods: (1) the first one is based on the measurement of the position of I-S (001/002) and (002/003) reflections (Środoń, 1980) before and after glycolation. The second one is found on the morphology of I-S (001) reflection peak (Inoue et al., 1989) after glycolation. Besides, semi-quantitative XRD bulk rock and insoluble residue analyses were performed on few representative samples.

Scanning Electron Microscopy (SEM) and petrophysical properties

To ensure the homogeneity of the petrographic characteristics of all the samples studied, we made SEM characterization of micrite microtexture on fresh surfaces, without acid attack, and after gold plating, and we measured the petrophysical properties (porosity and permeability) from plugs obtained from the same samples. Water porosimetry was performed to quantify total porosity (connected porosity) using Archimedes method (Richard et al., 2007, Cavailhes et al., 2013). Plugs were first dried in an oven at 60°C until they reached a stable mass (m_d) and then put upright in an airtight enclosure for 24 hours. at room temperature under vacuum at 2.6 Pa. They were progressively imbibed from their base with degassed deionized water, under a dynamic vacuum. The total porosity ϕ (%) is given by: $\phi = [(m_1 - m_d) / (m_1 - m_2)] \times 100$, where m_1 is the mass of the sample saturated with water and m_2 is the mass of the sample saturated with water weighed under water (hydrostatic underwater weighing). Permeability measurements (K) were performed on the same plugs with a gas permeameter equipped with a Hassler cell using nitrogen and the steady state flow method. They were made under an effective pressure of 0.1 MPa and then corrected for the Klinkenberg effect using a graphical method (Zinsner & Pellerin, 2007; Cavailhes et al., 2013). They are given here in millidarcy (mD).

$\delta^{13}C$, $\delta^{18}O$, Δ_{47} measurements

Eight samples have been analyzed for their stable isotope composition. These samples have been chosen as representative of each of the three studied areas (domain A, B and C of figure 1), based on petrographic observations and clay mineralogy data that were acquired prior to stable isotope measurements. The required amount of carbonate for replicate Δ_{47} measurements of the same sample (between 2 and 4 replicate analyses here; i.e., ~ 20 mg) was collected with a dental drill on the same plugs used for petrophysical measurements and SEM characterization. Measurements of Δ_{47} composition of carbonate samples were performed at Institut de Physique du Globe de Paris (IPGP, Stable Isotopes Team) using a Thermo Scientific MAT 253 gas-source mass spectrometer. Carbon, oxygen and clumped isotopes data were simultaneously acquired on gaseous CO_2 released after reaction of ~ 5 mg of carbonate powder in 104% phosphoric acid at 90°C (20 min in a common acid bath). The methods used for carbonate digestion, CO_2 purification, mass spectrometric measurements and data correction and standardization follow the procedure detailed by Bonifacie et al. (2017) and Katz et al. (2017), and includes two kinds of standards : i) gaseous CO_2 equilibrated at 25 and 1000°C and ii) homogenous carbonate powders (with a 1:1 ratio for unknown samples/standards).

$\delta^{18}O$ and $\delta^{13}C$ of the carbonate samples are expressed in per mil with respect to the VPDB standard. To guarantee the accuracy of the Δ_{47} data, we routinely analyzed two carbonate reference materials (IPGP-Carrara marble and 102-GCAZ01b, also reported by Dennis et al., 2011 and many other studies). The Δ_{47} values obtained for these carbonate standards over the course of this study (July 2014–May 2016) are: Δ_{47} = 0.412 ± 0.016‰ (1SD, n = 28) for IPGP-Carrara marble; Δ_{47} = 0.721 ± 0.020‰ (1SD, n = 21) for 102-GC-AZ01b. Finally, the corrected Δ_{47} values were converted into temperatures using the composite Δ_{47}-T calibration determined for all carbonate minerals for the 0–300°C temperature range (i.e., Eq. (3) from Bonifacie et al., 2017 that compiles 103 mean Δ_{47} data from seven different laboratories and with proper error propagation, which is $\Delta_{47} = 0.0422 * 10^6/T + 0.2182$ in the 25 °C acid digestion frame).

Parameterization of the kinetic models

Extracting thermal history information from kinetic paleothermometers is best treated with a forward approach, meaning that from quantitative observations in a given sample, such as a clumped isotope temperature or a vitrinite reflectance, we select preferred time-temperature history that would best reproduce all the measured paleothermometric data. These relationships can be simulated through a mathematical (forward) model representing the time-temperature dependence of the employed paleothermometric technique over geological time. This approach gains a particular interest when different paleothermometers are simultaneously employed, because each method acts with its own kinetic response to the inferred thermal history.

In this study, two distinct prograde thermal history paths, previously proposed by Butler, (1991) were used as an initial scenario to drive the different kinetic models. Furthermore, in order to consider mid-temperature scenarios, we also integrated five

additional time-temperature paths by adjusting the maximal burial temperature from 80 to 180°C. We computed the expected changes in vitrinite composition, Δ_{47} temperatures and % illite in I-S with time and temperature, for comparison with the measured values. Three empirical kinetic models were used with sequential time-temperature steps of 1Ma: (1) Vitrinite maturation was predicted by the Easy% Ro kinetic model of Sweeney & Burnham, 1990; (2) The extent of solid-state C-O bond reordering over time was simulated using the Δ_{47} kinetic model of Henkes et al. (2013) (see Shenton et al. 2015 for an application); and (3) the extent of smectite to illite conversion in I-S was calculated following the kinetic model of Huang et al., 1993.

The convergence criteria between measured data *versus* model predictions were iteratively defined to minimize: (1) the discrepancy between the whole dataset obtained by the mean of three independent paleothermometers (%illite in I-S, Ro% and TΔ_{47}), and (2) the gap between the measured data for each paleothermometer and the values computed mathematically for each proxy (%illite in I-S, Ro% and TΔ_{47}), given the different time-temperature paths to evaluate. A good match between data and models was observed by considering typical errors of ±0.1% for Ro%, ±10-15°C for TΔ_{47} and ±10% for %illite in I-S.

RESULTS

The semi-quantitative XRD bulk rock analyses showed that the studied limestone unit is mostly composed by calcite (>95%) with a minor proportion of clay minerals (<5%) including glauconite in some samples. XRD analyses on HCl-insoluble fraction revealed trace concentration of quartz, opal CT and K-feldspars. Table 1 shows the results of the mineralogical, petrographic, petrophysical and geochemical analyses of the clay and carbonate components from the investigated limestone unit.

Clay mineralogy

Clay mineralogyl results are presented in figure 2, where the relative proportions of the different minerals identified in the samples from the eighteen sampled sections are reported. From top to base are presented the results from sections located respectively in the external and internal domains (A, B, C) of the Bauges and Bornes massifs. In the studied area, clay minerals include illite, illite/smectite mixed-layers (I-S), chlorite, chlorite/smectite mixed-layers (C-S) and some kaolinite. Small quantities of quartz occur in the clay fraction of all samples. Three types of clay mineral assemblages are distinguished, depending on the geographical location of the samples (c.f. A, B and C domains). The first type (Sections A1 to A8) refers to clay mineral assemblages largely dominated by illite/smectite mixed-layers expanding to 17 Å after glycolation and therefore corresponding to I-S R0 ordering scheme (Fig. 3). They are associated with illite and occasionally with small amounts of C-S and kaolinite. The second type of clay mineral assemblages (Sections B9 to B13) is characterized by higher percentages of illite, a decreasing proportion of I-S, and the systematic occurrence of chlorite and C-S. In samples from the B domain, the proportion of illitic sheets in I-S

increases, and these I-S now mostly correspond to R1 ordering scheme. The last type (Sections C14 to C18) shows higher proportions of chlorite and illite, a lower amount of I-S with more than 90% illite layers, now corresponding to R3 ordering scheme (Fig. 3).

Micro-textural and petrophysical properties of the carbonate fraction

SEM characterization of micrites microtexture revealed very comparable and homogeneous properties among all samples (Fig. 5). The micritic particles are essentially anhedral, compact, with fully coalescent, though distinct, contacts (Deville de Periere et al., 2011, Régnet et al 2014). A relevant crystallography parameter, defined as the median of the maximum 2D particle lengths measured on SEM photomicrographs, varies between 1.30 and 1.45µm, and corresponds to fine micrites granulometry (0.5-2µm). Porosity and permeability measurements out of 58 samples exhibit very homogeneous values; i.e. porosity between 0.40% and 1.36% and permeability lower than 0.0001mD. No significant geographic variation was detected, both in term of petrographic texture and petrophysical properties (Table 1). These results suggest that the carbonate fraction from the investigated sections is not composed by differently sourced particles mixed together and did not experience distinctive recrystallization events.

Stable isotope composition of micrites ($\delta^{18}O_{carb}/\delta^{13}C_{carb}/\Delta_{47}$)

The stable isotopes data ($\delta^{18}O_{carb}/\delta^{13}C_{carb}/\Delta_{47}$) acquired on eight samples collected in the three different geographical domains (A, B and C) are reported in Table 1 and illustrated with different colors in the cross plots of Figure 5. Despite the fact that the samples were collected in different localities tens of kilometers apart, they all exhibit small ranges of variations in $\delta^{18}O_{carb}$ (between -3.15‰ and -3.89‰; n=8 samples) and $\delta^{13}C_{carb}$ (from 1.6‰ to 2.90 ‰; n=7 – sample A1 is offset with a $\delta^{13}C_{carb}$ = 0.04‰). This small range of variation likely reflects the fact that all samples precipitated (or recrystallized) in comparable environmental conditions (i.e., temperature, oxygen isotope composition of the parent fluid, water to rock ratios).

The Δ_{47} values of the samples investigated here are varying between 0.634‰ and 0.400‰. The external reproducibility out of 2 to 4 replicate analyses of the same micrite powder ranges between ±0.010‰ and ±0.049‰ (± 1 S.D., with one offset for sample B12 ±0.076‰; Table 1). This is larger than the external reproducibility obtained in this study on homogeneous standards (± 0.018‰, n=49) and likely reflects the relative isotopic heterogeneity of the micrite samples investigated here (compared to homogeneous standards). In contrast with the regional-scale homogeneity on $\delta^{18}O_{carb}$ and $\delta^{13}C_{carb}$ compositions of the micrites from all investigated geographical domains, Δ_{47} values from carbonate samples from the C domain are significantly different from the two other domains. The Δ_{47} values of the C domain are averaging at 0.421±0.015‰ (n=4 samples and 11 analyses in total), which is within the uncertainties on the Δ_{47} values found for calcite marbles (Bonifacie et al., 2013; see for example Carrara marble analyzed as a standard in this study with Δ_{47} = 0.412±0.016‰,

1SD, n = 28 analyses). On the other hand, the Δ_{47} values found for domain A and B are indistinguishable from each other (respectively of 0.615±0.025‰ and 0.623±0.015‰, n=2 samples for each domain, 11 analyses in total). Given the fact that the four samples collected from the A and B domains display $\delta^{18}O_{carb}$, $\delta^{13}C_{carb}$ and Δ_{47} values that are all indistinguishable when respective uncertainties are considered, their stable isotope compositions are averaged in the following discussion. The Δ_{47} values are distributed in two clusters with corresponding temperatures averaging at 183±17°C for the C domain and 51±8°C for the A and B domains (Table 1).

Table 1 also presents the oxygen isotopic compositions of the water ($\delta^{18}O_{water}$) in equilibrium with the carbonate that can be calculated using both the $T\Delta_{47}$ and the $\delta^{18}O_{carb}$ values measured as well as the oxygen isotope fractionation between calcite and water from Watkins et al. (2013). For samples of the A and B domains, the calculated $\delta^{18}O_{water}$ are averaging at 1.7±1.2‰ (1 S.D.; n=4), i.e., enriched in ^{18}O compared to expected Late Cretaceous seawater ($\delta^{18}O_{water}$ ~-1‰ ; Jenkyns et al. 1994). Contrastingly, for the C domain, the calculated oxygen isotope composition of the fluid in equilibrium with the micrite samples are way more enriched in ^{18}O, with $\delta^{18}O_{water}$ averaging at 17±1‰ (1 S.D.; n=4) – that is hard to reconcile with known $\delta^{18}O_{water}$ of crustal fluids in carbonate settings (e.g., Karhaka et al. 2003). [It is noteworthy that Dassié et al. (2018) recently showed that $\delta^{18}O_{water}$ values directly measured in fluid inclusions from diagenetic cements and the $\delta^{18}O_{water}$ independently calculated from the Δ_{47} and $\delta^{18}O_{carb}$ data, within the same cements, agree within 1‰. These findings demonstrate the viability of coupling Δ_{47} and $\delta^{18}O_{carb}$ for determining the $\delta^{18}O_{water}$ of the mineralizing fluid, at least in absence of solid-state diffusion].

Organic matter maturity

The "sublithographic limestones" do not contain organic matter. However, thermal maturity data of organic matter bearing rocks from several locations and different stratigraphic intervals of the northern subalpine chains have been previously published. These data come either from vitrinite reflectance (Ro%) measurements (Kübler et al. 1974; Kisch, 1980; Gorin & Monteil, 1990 ; Moss 1992; Schegg, 1992a,b; Deville & Sassi, 2006) or from Rock-Eval pyrolysis analyses (Gorin et al. 1989; Gorin & Monteil; 1990). Here we have chosen to integrate and discuss only the dataset of Gorin & Monteil, (1990), because organic matter analyses were completed on the Maastrichtian Wang formation (Stacher, 1980; Villard 1988) which directly overlies the "sublithographic limestones" (Fig. 2). These authors showed that in the northern subalpine massif, the Maastrichtian Wang formation has reached a wide range of maturities (Table 1). Vitrinite reflectance Ro ranges from 0.45 ± 0.05% to 0.55 ± 0.05% in the area covered by the A domain (corresponding to A1 and A6 samples of this study), is equal to 0.7 ± 0.1% in the B domain (B9 sample of this study) and increases up to 1.3 ± 0.2% in the C domain (C16 and C17 samples of this study). Rock-Eval 2 pyrolysis data confirm this trend of organic matter maturity and reveal that oil window was reached in the

eastern domain C (T_{max}>460°C), whereas OM remains immature (T_{max}<430°C) in the western domain A and B of the subalpine massifs (Gorin & Monteil, 1990).

DISCUSSION

Thermal evaluation recorded by clay minerals and organic matter

In the western part of the studied Bauges and Bornes massifs (domain A of figure 1), the clay assemblages of the Upper Cretaceous "sublithographic limestones" are largely dominated by I-S of R0 type. The frequent occurrence of these minerals, also found in the underlying Lower Cretaceous formations, indicates that the thermal influences are very weak (Deconinck et al., 1985). Indeed, smectite illitization processes are known to take place when temperatures reache about 60-70°C (Środoń & Clauer , 2001; Środoń et al., 2009; Thyberg et al., 2010), though these values also depend on lithology and were mainly apply to argillaceous rocks and volcanic ashes layers (Šucha et al., 1993). Therefore, the clay mineralogy suggests that the westernmost domain A did not undergo temperatures above 70°C. Since the influence of thermal diagenesis is negligible in the western part of the subalpine massifs, clay mineral sedimentation was possibly dominated by I-S R0 which can be assimilated to smectites. This result is in line with findings from Upper Cretaceous deposits from numerous sedimentary basins, where smectites dominate the sedimentation record (Jeans et al., 2001; Deconinck et al., 2005; Chenot et al., 2018). The negligible influence of thermal diagenesis highlighted by clay assemblages in the western part of the study area, is in agreement with the low T_{max} values (T_{max}≤430°C; Gorin & Monteil, 1990) and with the vitrinite reflectance values (0.45% to 0.55%) pointing at an immature organic matter. Conclusively, all the available paleo-thermicity proxies suggest that the western part (A domain) of the subalpine massifs (Bauges and Bornes) did not experience burial temperature above 70-80°C (Fig. 7).

In the eastern part (C domain) of the studied subalpine massifs, the clay mineral assemblages are dominated by chlorite, illite and I-S R3 containing a small proportion (mostly below 10%) of smectite sheets. This type of assemblage results from the illitization of I-S R0 through smectite dissolution/precipitation processes (Nadeau et al., 1985) and from the transformation of these smectitic minerals into chlorite. The C-S present in the eastern sections are likely the intermediates of smectite to chlorite transformations. The difference in the composition of clay assemblages between the western and the eastern part of the subalpine massifs was already noticed and interpreted as due to tectonic overload triggered by the prealpine nappes (Deconinck & Debrabant, 1985). New data provided in this study suggest that samples from the C domain likely experienced maximum temperatures up to 140°C, confirming that thermal diagenesis was responsible for the illitization and chloritization of I-S R0 (Fig. 7), the increase of vitrinite reflectance (up to 1.3%) and of Rock-Eval T_{max} (T_{max}>460°C) in these localities. The relationship observed in the studied area between the Rock-Eval T_{max} and the illite content in illite-smectite (I-S) mixed layers agrees with the one observed by Dellisanti et al. (2010) in similar syn-orogenic successions from the Northern Apennines (Italy). These results are also concordant with the maximum burial temperature of

180°C estimated in the studied area by Butler, (1991).

Samples from the B domain show an intermediate clay mineral assemblage with the occurrence of I-S R1 and incipient chloritization of I-S R0, associated with values of vitrinite reflectance (~0.7%) and T_{max} (~437°C) pointing at moderate maturity . Altogether, clay minerals and organic maturity data indicate that the B domain experienced a moderate thermal influence compared to the external and internal domains (A and C, respectively).

Effects of lithology on clay mineral diagenesis

Although the investigated lithology consists of a micritic limestone with a $CaCO_3$ content of up to 95%, and potassium deficiency, the illitization processes described in this study are comparable to those described in argillaceous rocks or ashes layers, confirming that temperature is the dominant controlling factor at regional scale (Środoń & Clauer, 2001). However, in the B and C domains, chloritization processes are progressively increasing from West to East where and the chlorite proportion reaches 50% of the clay fraction. Such chlorite proportions cannot be explained by depositional heterogeneities linked to detrital input. Indeed, the hot and hydrolyzing climates dominating the Late Cretaceous time did not allow chlorite preservation. Furthermore, in the absence of diagenetic transformations, the chlorite proportions are always very low in Upper Cretaceous sediments (Jeans et al., 2001; Deconinck et al., 2005). The chloritization processes in the studied carbonate succession were probably favored by the magnesium release from the transformation of High-Magnesium Calcite (HMC) into Low-Magnesium Calcite (LMC) during diagenesis. This process is particularly evident in marl-limestone alternations of the subalpine ranges where I-S R0 evolved into illites within the marls and into chlorites within the limestones (*e.g.* Deconinck & Chamley, 1983, Ferry et al., 1983; Deconinck & Debrabant, 1985; Levert & Ferry, 1988).

Interpretation of stable isotope data of micrites

In the studied sublithographic limestones, the micrite samples record contrasting Δ_{47} temperatures clustered in two distinct groups, depending on their geographic locations. The micrites from the A and B domains have $T\Delta_{47}$ clustered at 51±8°C (n=4 samples) which sharply contrast with the micrites from the more internal C domain, displaying $T\Delta_{47}$ clustered at 183±17°C (n=4 samples). Given the fact that all the investigated micritic calcites from all domains show very similar micro-texture, petrophysical properties, as well as $\delta^{13}C$ and $\delta^{18}O_{carb}$ isotopic compositions (Fig.4, 5 and Table 1), it is unlikely that this sharp difference in $T\Delta_{47}$ values could result from different recrystallization events. We suggest that the high temperatures recorded in samples of the eastern C domain result from ^{13}C-^{18}O bonds re-equilibration via solid-state diffusion at temperatures higher than the blocking temperature. Such hypothesis also finds support in the fact that: (1) the calculated $\delta^{18}O_{water}$ of about 19‰ for micrites of the C domain are too high to be reconciled with the most common $\delta^{18}O_{water}$ of diagenetic fluids in sedimentary basins (Karhaka et al. 2003); (2) clay mineral and vitrinite reflectance data indicate a maximal burial temperature up to 160-180°C for this area.

Following the kinetic model of Henkes et al. 2013, such temperature conditions can lead to a fully-re-equilibration of Δ_{47} compositions.

It is noticeable that the observed $\delta^{18}O_{carb}$ composition of micrites are slightly depleted in ^{18}O compared to carbonates precipitated in equilibrium with Late Cretaceous shallow seawater (see light grey box in Figure 5; Veizer et al. 1999). However, the micrite oxygen and carbon isotopic compositions are comparable to those observed in analogue deep-chalk sediments with similar facies (e.g. $\delta^{18}O_{carb}$ between -1.5 and -3‰ for Upper Cretaceous chalk deposits from different areas; Jenkyns et al. 1994 and Schiinfeld et al. 1991; black box in Figure 5). This suggests that all the micrites from this study likely recrystallized at higher temperatures than the original one at depositional site. Such hypothesis finds support in two observations. First, the limestone units, initially composed of calcareous ooze with planktonic foraminifera and coccoliths fragments, now exhibit numerous petrographic hints of recrystallization (i.e. particle shapes, type of contact between grains and crystallometry parameters). Second, the measured $T\Delta_{47}$ show higher temperatures than coeval shallow seawater (i.e., 20-26°C following Jenkyns et al. 1994). Noticeably, the $T\Delta_{47}$ of micrite samples from the external domains (A and B), not affected by Δ_{47} resetting, point toward a recrystallization event occurring during shallow burial, at temperatures close to 50°C and by fluids with $\delta^{18}O_{water}$ values of +1.7±1.2‰. Such recrystallization event may correspond to the transformation of the metastable High-Magnesium Calcite (HMC) into Low-Magnesium Calcite (LMC) of the micritic sediment (Schlager & James, 1978).

Overall, the micrite samples investigated here exhibit apparent $T\Delta_{47}$ values that are expected to be an integration of: (1) temperature, timing, and extent of the shallow burial recrystallization occurring for all geographic domains (A, B and C) and (2) an additional overprint by solid-state C-O bond reordering only in samples from the C domain, which was function of the thermal history and of specific C-O bond reordering kinetics of Δ_{47} compositions.

Forward thermal modeling approach (Δ_{47}, Ro% and %I in I-S mixed layer)

Guided by the paleothermometric results acquired on three samples representative of the three geographic domains investigated in this study, we employed a forward modeling approach to find the best thermal scenario to reconcile all the obtained Δ_{47}, vitrinite reflectance and clay mineral data. This approach is devoted to refine the burial and exhumation history of the sampled areas. The model results are shown in Figure 7 where seven different time-temperature scenarios, with varying maximal burial temperature (MBT) are considered. These scenarios are: (1) pre-thrusting burial (88-65Ma); (2) Eocene inversion (65Ma-45Ma); (3) main emplacement of thrust units and associated heat increase (40Ma to 8Ma); and (4) erosion (8Ma-present).

First of all, the results of the forward models for each paleothermometric proxy, demonstrate that model predictions and data may converge for a set of thermal histories (TH)

with maximal burial temperature (MBT) ranging from 60°C to 180°C. More specifically, given the measured Ro%, Δ_{47} and % illite in I-S mixed layer for the three selected samples (c.f. A1, B9 and C16 samples), the forward modeling results predict that:

TH1-TH2 (MBT between 60°C and 80°C) are the most likely scenarios suggested for A1 sample (A domain) because these time-temperature paths are the only ones prone to generate a substantial agreement between all the available paleothermometric data. As discussed previously, sample A1 exhibits a $T\Delta_{47}$ of 61±15°C suggesting a recrystallization event under shallow burial temperatures, without any record of the successive solid-state diffusion overprint. In this case, Δ_{47} thermometry only preserves a screenshot of punctual recrystallization temperature and does not provide important information on the sample thermal history. The weak maturity recorded for the A domain by vitrinite reflectance data (R_o%: 0.45±0.05) correlated with a low %illite (:25±4%) in I-S mixed-layers, and is also in good agreement with TH1-TH2 model prediction, suggesting that A1 sample likely experienced maximum burial temperature in the range 60-80°C.

Following the same model predictions, it comes out that mid-scenarios TH3- TH4, with MBT between 100 and 120°C, are the most susceptible scenarios to conjointly increase the illite content in I-S (between 51 to 93 %illite) and vitrinite reflectance (between 0.55 to 0.67%), without providing sufficient activation energy to initiate Δ_{47} kinetic C-O bond reordering. The paleothermometric data available for sample B9 (c.f., R_o%: 0.7±0.1; I% in I-S:48±9% and $T\Delta_{47}$:54±9°C) from the B domain agree perfectly with model predictions for TH3-TH4. Therefore, sample B9 likely experienced maximal burial temperatures ranging from 100 to 120°C.

Finally, sample C16 from the C domain exhibits $T\Delta_{47}$ in excess of 120°C compared to samples A1 and B9, a clear increase of vitrinite reflectance values (Ro% = 1.3±0.2) and a near total illitization of I-S mixed layer (up to 90% illite). These data clearly indicate a significantly higher level of thermal maturity in the C domain. First, Δ_{47} data in sample C16 have been previously interpreted as reflecting the attainment of Δ_{47} blocking temperatures reached during the cooling stage (i.e. from 8Ma to present-day), that followed a complete re-equilibration of Δ_{47} compositions at maximal burial temperatures (see Fig.7.B for more detail). Δ_{47} kinetic modeling results showed that only TH7 (maximal burial temperature >180°C), or hotter scenarios, may provide sufficient activation energy to generate the observed complete re-equilibration of Δ_{47} in C16 samples. This finding is a strong argument in favor of maximum burial temperatures higher than 180°C in this area. Then, the available Ro% values and the near complete illitization of I-S mixed layer observed in C16 sample, also showing a substantial agreement with TH7 modeling predictions, conclusively point toward a temperature regime with maximum temperature close to 180°C.

Guided by the data-model comparisons presented on three representative samples of the studied area, we provide quantitative information on paleotemperatures and, indirectly, on sample burial and exhumation histories. In light of these results, it is clear that samples

collected from the same stratigraphic interval (Upper Cretaceous "sublithographic limestones"), and from closed geographic areas, may have experienced very contrasting thermal histories, with maximum burial temperatures varying from 60-80°C in the western external domains (A and B), up to 180°C in the internal domain (C) of the studied area. These heterogeneities in the paleothermal record may reflect significant changes in overburden, induced by the emplacement of thrust-sheet units with variable thickness. Indeed, by considering a regional geothermal gradient of 25±5 °C/km for the time encompassing tectonic loading and exhumation (Schegg, 1992b), the paleothermometric data suggest that the prealpine nappes, presently eroded, were 4-7 km and 1.3-2km thick in the eastern and western domains, respectively. These results are consistent with previous estimation of Deville & Sassi (2006) who calculated that more than 4-6 km of prealpine nappes was thrust in the North-West of the studied area. However, we cannot rule out that the East to West increase in paleotemperatures, recorded in this study, may also reflect an heat flow increase without significant additional burial. The definition of the precise process causing this temperature gradient is beyond the scope of this study and would require in-depth thermokinematic modeling to be addressed.

CONCLUSIONS

The three proxies (i.e. clay diagenesis, organic matter maturity and carbonate clumped isotope composition) used to reconstruct the thermal history of an Upper Cretaceous limestone unit from the northern subalpine domain (Bauges and Bornes massifs, northern French Alps) provided a coherent dataset showing the existence of a prograde diagenetic gradient from West to East, notably due to the tectonic emplacement of the prealpine nappes. Although the studied sediments correspond to micritic limestones, clay mineral diagenesis is expressed, similarly to what is expected for argillaceous rocks, by the progressive illitization of smectites. The degree of illitization makes it possible to identify three mineralogical zones within the studied massifs: a western zone where sedimentary I-S R0 are preserved, suggesting that the burial temperatures never exceeded 70°C; an intermediate zone marked by the presence of I-S R1, indicating burial temperatures in the range 100-120 °C; and an eastern zone marked by the presence of I-S R3, indicating temperatures in the order of 160 to 180°C. Organic matter maturity data (from T_{max} and Ro%) are consistent with the clay mineral dataset, pointing at an immature organic matter in the western part of the subalpine massif and a prograde increase of T_{max} and Ro% values toward the East. The low Δ_{47} temperatures recorded in micrite samples from the western area of the subalpine massifs are in excess of ~20°C of plausible depositional temperatures, suggesting that micrite recrystallized at such temperatures. However, in the eastern part of the massifs, four samples collected 30km apart, exhibit Δ_{47} temperatures of ~180°C that is a clear evidence of a regional-scale solid-state re-ordering process, allowing to apply the newly developed Thermal History Reordering Model (THRM; Henkes et al. 2014). Altogether, the paleothermometric data presented in this study, combined with the results of forward thermal modeling, allow to propose thermal scenarios suggesting that the thickness of the prealpine nappes was between 4 and 7 km and between 1.3 to 2 km in the inner and outer parts of the subalpine massifs, respectively.

REFERENCES

AI AASM, I.S. & VEIZER, J. (1986) Diagenetic stabilization of aragonite and low-Mg calcite, 1. Trace elements in rudists. *Journal of Sedimentary Petrology*, 56, 138-152.

ALDEGA, L., CORRADO, S., GRASSO, M., & MANISCALCO, R. (2005). Correlation of Inorganic and Organic Thermal Indicators in the Eastern Sicily Fold-and-Thrust Belt. *Atti Ticinensi Di Scienze Della Terra*, *10*, 61–65.

BELLAHSEN, N., MOUTHEREAU, F., BOUTOUX, A., BELLANGER, M., LACOMBE, O., JOLIVET, L. & ROLLAND, Y. (2014) Collision kinematics in the western external Alps. *Tectonics*, 33, 1055-1088.

BENNETT, C. E., WILLIAMS, M., LENG, M. J., LEE, M. R., BONIFACIE, M., CALMELS, D., FORTEY, R.A., LAURIE, J.R., OWEN, A. W., PAGE A.A., MUNNECKE A. & VANDENBROUCKE, T.R.A. (2018) Oxygen isotope analysis of the eyes of pelagic trilobites: testing the application of sea temperature proxies for the Ordovician. *Gondwana Research,* 57, 157-169

BERGMAN, S.C., HUNTINGTON, K.W. & CRIDER, J.G. (2013) Tracing paleofluid sources using clumped isotope thermometry of diagenetic cements along the moab fault, Utah. *Am. J. Sci*., 313, 490–515.

BONIFACIE, M., CALMELS, D., EILER, J.M., HORITA, J., CHADUTEAU, C., VASCONCELOS, C., AGRINIER, P., KATZ, A., PASSEY, B.H., FERRY, J.M. & BOURRAND, J.J. (2017) Calibration of the dolomite clumped isotope thermometer from 25 to 350 °C, and implications for a universal calibration for all (Ca, Mg, Fe)CO_3 carbonates. *Geochim. Cosmochim. Acta*, 200, 255–279.

BONIFACIE M., CALMELS D. & EILER J.M. Clumped isotope thermometry of marbles as an indicator of the closure temperatures of calcite and dolomite with respect to solid-state reordering of C–O bonds. *Goldschmidt Conference* (Florence, Italy), 2013.

BRISTOW, T.F., BONIFACIE, M., DERKOWSKI, A. EILER, J. M. & GROTZINGER, J.P. 2011 A hydrothermal origin for isotopically anomalous cap dolostone cements from south China. *Nature,* 474, 68-71.

BUDD, D.A., FROST, E.L., HUNTINGTON, K.W. & ALLWARDT, P.F. (2013) Syndepositional Deformation Features In High-Relief Carbonate Platforms: Long-Lived Conduits for Diagenetic Fluids. *J. Sediment. Res.,* 83, 12–36.

BUTLER, R. W. H. (1991) Hydrocarbon maturation, migration and tectonic loading in the western Alpine foreland thrust belt, in W. A. England and A. J. Fleet, eds., Petroleum migration: *Geological Society Special Publication (London)*, 59, 227– 244.

CAVAILHES, T., SIZUN J.-P., LABAUME, P., CHAUVET, A., BUATIER, M., SOLIVA, R., MEZRI, L., CHARPENTIER, D., TRAVÉ, A. & GOUT, C., 2013. Influence of fault rock foliation on fault zone permeability: The case of deeply buried arkosic sandstones (Grès d'Annot, SE France). *AAPG Bull*., 97, 1521–1543.

CHENOT E., DECONINCK JF., PUCEAT E., PELLENARD P., GUIRAUD M., JAUBERT M., JARVIS I., THIBAULT N., COCQUEREZ T., BRUNEAU L., RAZMJOOEI M.J., BOUSSAHA M., RICHARD J., SIZUN J.P. & STEMMERIK L. (2018) Continental weathering as a driver of late Cretaceous cooling: new insights from clay mineralogy of Campanian sediments from the southern Tethyan margin to the boreal realm. *Global and Planetary Change*, 162, 292-312.

CZERNIAKOWSKI, L.A., LOHMANN, K.C. & WILSON, J.L. (1984) Closed-system marine burial diagenesis: isotopic data from the Austin Chalk and its components. *Sedimentology*, 31, 863-877.

DALE, A., JOHN, C.M., MOZLEY, P.S., SMALLEY, P.C., MUGGERIDGE, A.H. (2014)

Time-capsule concretions: Unlocking burial diagenetic processes in the Mancos Shale using carbonate clumped isotopes. *Earth Planet. Sci. Lett.,* 394, 30–37.

DASSIE E. GENTY, D., NORET, A., MANGENOT, X., MASSAULT, M., LEBAS, N., DUHAMEL, M., BONIFACIE, M., GASPARRINI, M., MINSTER B., AND MICHELOT, J.L. (2018) A newly designed analytical line to examine the reproducibility of fluid inclusion isotopic compositions in small carbonate samples. *G3, Geochemistry, Geophysics, Geosystems,* 19, 1-16

DECONINCK J. F. & CHAMLEY H. (1983) Héritage et diagenèse des minéraux argileux dans les alternances marno-calcaires du Crétacé inférieur du domaine subalpin. *C. R. Acad. Sc.*, Paris, 297, 589-594.

DECONINCK J.F., AMEDRO F., BAUDIN F., GODET A, PELLENARD P., ROBASZYNSKI F., & ZIMMERLIN I. (2005) Late Cretaceous palaeoenvironments expressed by the clay mineralogy of Cenomanian to Campanian chalks from the East of the Paris Basin (Craie 700 program). *Cretaceous Research*, 26, 171-179.

DECONINCK J. F., BEAUDOIN B., CHAMLEY H., JOSEPH P. & RAOULT J. F. (1985).- Contrôles tectonique, eustatique et climatique de la sédimentation argileuse du domaine subalpin français au Malm-Crétacé. *Rev. Géol. Dyn. Géogr. Phys.,* 26, 311-320.

DECONINCK, J.F. & DEBRABANT, P. (1985) Diagenèse des argiles dans le domaine subalpin: rôle respectif de la lithologie, de l'enfouissement et de la surcharge tectonique. *Revue de géologie dynamique et de géographie physique,* 26 (5), 321-330.

DELAMETTE, F., CHAROLLAIS, J., DECROUEZ, D. & CARON, M. (1997) Les grès verts helvétiques (Aptien moyen-Albien supérieur) de Haute-Savoie, Valais et Vaud. *Publication du département de Géologie-Paléontologie de l'Université de Genève,* 23*,* 400pp.

DELLISANTI, F., PINI, G.A., BAUDIN, F., 2010. Use of T_{max} as a thermal maturity indicator in orogenic successions and comparison with clay mineral evolution. *Clay minerals* 45, 115-130.

DENNIS, K.J., AFFEK, H.P., PASSEY, B.H., SCHRAG, D.P. & EILER, J.M. (2011) Defining an absolute reference frame for "clumped" isotope studies of CO_2. *Geochim. Cosmochim. Acta*, 75, 7117–7131.

DENNIS, K.J. & SCHRAG, D.P.(2010) Clumped isotope thermometry of carbonatites as an indicator of diagenetic alteration. *Geochim. Cosmochim. Acta*, 74, 4110–4122.

DEVILLE DE PERIERE, M., DURLET, C., VENNIN, E., LAMBERT, L., BOURILLOT, R., CALINE, B. & POLI, E. (2011) Morphometry of micrite particles in cretaceous microporous limestones of the Middle East: Influence on reservoir properties. *Mar. Pet. Geol*., 28, 1727–1750.

DEVILLE, E. & SASSI, W. (2006) Contrasting thermal evolution of thrust systems: An analytical and modeling approach in the front of the western Alps. *Am. Assoc. Pet. Geol. Bull.,* 90, 887–907.

ENOS, P. (1986) Diagenesis of mid-Cretaceous rudist reefs, Valles platform, Mexico. In: Reef Diagenesis. J.H. Schroeder & B.H. Purser (eds), *Springer-verlag, Berlin*, 160-185.

ESPITALIÉ, J., DEROO, G. & MARQUIS, F., 1985. La pyrolyse Rock-Eval et ses applications. Rev. I. fr. Pétrole 40, 563e579.

FAY-GOMORD O., ALLANIC C., WOUTER S., HONLET R., CHAMPENOIS F., BONIFACIE M., CHADUTEAU C., MUCHEZ P., VERBIEST M., LASSEUR E., SWENNEN R. Understanding fluid-flow during tectonic reactivation: an example from the flamborough head chalk outcrop (UK) *Geofluids.*

FERRY S. COTILLON P. & RIO M. (1983) Diagenèse croissante des argiles dans les niveaux isochrones de l'alternance calcaire-marne valanginienne du basin vocontien. Zonation géographique. *C.R. Acad. Sci. Paris*, 297, 51-56.

GHOSH, P., ADKINS, J., AFFEK, H., BALTA, B., GUO, W., SCHAUBLE, E. A., SCHRAG, D. & EILER, J.M. (2006b). $^{13}C–^{18}O$ bonds in carbonate minerals: A new kind of paleothermometer. *Geochim. Cosmochim. Acta*, 70, 1439–1456.

GORIN, G. E., & E. MONTEIL. (1990) Preliminary note on the organic facies, thermal maturity and dinoflagellate cysts of the upper Maastrichtian Wang Formation in the northern Subalpine massifs (western Alps, France). *Eclogae Geologicae Helveticae*, 83, 265–285.

GORIN, G., F. GULACAR. & Y. CORNIOLEY. (1989) Organic geochemistry, maturity, palynofacies and palaeoenvironment of upper Kimmeridgian and lower Tertiary organic-rich samples in the southern Jura (Ain, France) and Subalpine massifs (Haute-Savoie, France). *Eclogae Geologicae Helveticae*, 82, 491–515.

GORIN, G.E. & MONTEIL, E. (1990) Preliminary note on the organic facies, thermal maturity and dinoflagellate cysts of the Upper Maastrichtian Wang Formation in the northern subalpine massifs (Western Alps, France). *Eclogae Geologicae Helvetiae,* 83, 265-285

HENKES, G. A., PASSEY, B.H., GROSSMAN, E.L., SHENTON, B.J., PEREZ-HUERTA, A. & YANCEY, T.E. (2014) Temperature limits for preservation of primary calcite clumped isotope paleotemperatures. *Geochim. Cosmochim. Acta*, 139, 362–382.

HENKES, G. A., PASSEY, B.H., WANAMAKER, A.D., GROSSMAN, E.L., AMBROSE, W.G. & CARROLL, M.L. (2013) Carbonate clumped isotope compositions of modern marine mollusk and brachiopod shells. *Geochim. Cosmochim. Acta*, 106, 307–325.

HONLET, R., GASPARRINI, M., JÄGER, H., MUCHEZ, P. & SWENNEN, R., 2017. Precursor and ambient rock paleothermometry to assess the thermicity of burial dolomitization in the southern Cantabrian Zone (northern Spain). *International Journal of Earth Sciences*, 0, 1-21.

HOWARD J.J. & ROY D.M. (1985) - Development of layer charge and kinetics of experimental smectite alteration. Clays and Clay Minerals, 33, 81-88.

HUANG, W.-L.W., LONGO, M.-J.J. & PEVEAR, D.-R.D. (1993) An experimentally derived kinetic model for smectite-to-illite conversion and its use as a geothermometer. *Clays Clay Miner.*, 41, 162–177.

HUNTINGTON, K.W., BUDD, D. A., WERNICKE, B.P. & EILER, J.M., 2011. Use of clumped-isotope thermometry to constrain the crystallization temperature of diagenetic calcite. *J. Sediment. Res.,* 81, 656–669.

INOUE, A., BOUCHET, A., VELDE, B. & MEUNIER, A. (1989) Convenient Technique for Estimating Smectite Layer Percentage in Randomly Interstratified Illite/Smectite Minerals. *Clays Clay Miner.*, 37, 227–234.

INOUE, A., KOHYAMA, N., KITAGAWA, R. & WATANABE, T. (1987) Chemical and morphological evidence for the conversion of smectite to illite. *Clays Clay Miner.,* 35, 111-120.

JEANS C.V., MITCHELL J.G., FISHER M.J., WRAY D.S. & HALL I.R. (2001) Age, origin and climatic signal of English Mesozoic clays based on K/Ar signatures. *Clay Minerals*, 36, 515-539.

JENKYNS, H. C., GALEF, A. S., & CORFIELD, R. M. (1994). Carbon- and oxygen-isotope stratigraphy of the English Chalk and Italian Scaglia and its palaeoclimatic significance. *Geol. Mag.* **131**, *1-34*

KATZ, A., BONIFACIE, M., HERMOSO, M. CARTIGNY, P. & CALMELS, D. (2017) Laboratory-grown coccoliths exhibit no vital effect in clumped isotope composition on a range of geologically relevant temperatures. *Geochim. Cosmochim. Acta*, 208, 335–353.

KELE, S., BREITENBACH, S.F.M., CAPEZZUOLI, E., MECKLER, A.N., ZIEGLER, M., MILLAN, I.M., KLUGE, T., DEAK, J., HANSELMANN, K., JOHN, C.M., YAN, H., LIU, Z. & BERNASCONI, S.M. (2015) Temperature dependence of oxygen- and clumped isotope fractionation in carbonates: A study of travertines and tufas in the 6-95°C temperature range. *Geochim. Cosmochim. Acta* 168, 172–192.

KELSON, J.R., HUNTINGTON, K.W., SCHAUER, A.J., SAENGER, C. & LECHLER, A.R. (2017) Toward a universal carbonate clumped isotope calibration: Diverse synthesis and preparatory methods suggest a single temperature relationship. *Geochim. Cosmochim. Acta,* 197, 104–131.

KISCH, H, J. (1980) Illite crystallinity and coal rank associated with lowest-grade metamorphism of the Taveyanne greywacke in the Helvetic zone of the Swiss Alps. *Eclogae Geol. Helv*., 73, 753–777.

KHARAKA, Y. K., & HANOR, J. S. (2007). Deep fluids in the continents: 1. Sedimentary basins. *Surface and Ground Water, Weathering and Soils. Book, Treatise on Geochemistry 5.*

KÜBLER, B. & JABOYEDOFF, M. (2000) Illite Cristallinity. *C. R. Acad. Sci. Paris,* 331, 75-89.

KUBLER, B., MARTINI, J. & VUAGNAT, M. (1974) Very low grade meatmorphism inthe Western Alps. *Sclnreizerische Mineralogische und Petrographische Mitteilungen*, 54, 461-469.

LAWSON, M., SHENTON, B.J., STOLPER, D.A., EILER, J.M., RASBURY, E.T., BECKER, T.P., PHILLIPS-LANDER, C.M., BUONO, A.S., BECKER, S.P., POTTORF, R., GRAY, G.G., YUREWICZ, D. & GOURNAY, J. (2017) Deciphering the diagenetic history of the El Abra Formation of eastern Mexico using reordered clumped isotope temperatures and U-Pb dating. *Geological Society of America bulletin*, 130, 1–13.

LEVERT J., & FERRY S. (1988) Diagenèse argileuse complexe dans le mésozoïque subalpin révélée par cartographie des proportions relatives d'argiles selon des niveaux isochrones. *Bull. Soc. Géol. Fr.*, 4, 1029-1038.

LOYD, S.J., CORSETTI, F. A., EILER, J.M. & TRIPATI, A. K. (2012) Determining the Diagenetic Conditions of Concretion Formation: Assessing Temperatures and Pore Waters Using Clumped Isotopes. *J. Sediment. Res*., 82, 1006–1016.

LOYD, S.J., DICKSON, J. A. D., SCHOLLE, P. A. & TRIPATI, A. K. (2013) Extensive, uplift-related and non-fault-controlled spar precipitation in the Permian Capitan Formation. *Sediment. Geol.,* 298, 17–27.

MANGENOT, X., BONIFACIE, M., GASPARRINI, M., GOETZ, A., CHADUTEAU, C., ADER, M. & ROUCHON, V. (2017) Coupling Δ47 and fluid inclusion thermometry on carbonate cements to precisely reconstruct the temperature, salinity and $\delta^{18}O$ of paleo-groundwater in sedimentary basins. *Chem. Geol*., 472, 44–57.

MANGENOT, X., GASPARRINI, M., ROUCHON, V. & BONIFACIE, M. (2018) Basin-scale thermal and fluid flow histories revealed by carbonate clumped isotopes (Δ_{47}) – Middle Jurassic carbonates of the Paris Basin depocentre. *Sedimentology*, 65, 123-150

MOLDOVANYI, E.V. & LOHMANN, K.C. (1984) Isotopic and petrographic record of phreatic diagenesis: lower Cretaceous Sligo and Cupido formations. *Journal of Sedimentary Petrology*, 54, 972-985.

MOORE, D.M. & REYNOLDS, R.C.J. (1997) X-Ray Diffraction and identification and analysis of clay minerals. *Oxford University Press*, 378pp

MOSS, S. J. (1992) Organic maturation in the French Subalpine chains: Regional differences in burial history and the size of tectonic loads. *Journal of the Geological Society (London*), 149, 503–515.

NADEAU P.H., WILSON M.J., MCHARDY W.J. & TAIT J.M. (1985) The conversion of smectite to illite during diagenesis: evidence from some illitic clays from bentonites and sandstones. *Mineralogical magazine*, 49, 393-400.

NADEAU, P.H., PEACOR, D.R., YAN, J. & HILLIER, S. (2002) I–S precipitation in pore space as the cause of geopressuring in Mesozoic mudstones, Egersund Basin, Norwegian continental shelf. *American Mineralogist*, 87, 1580–1589.

PAGEL M., BONIFACIE M., SCHNEIDER D.A., GAUTHERON C., BRIGAUD B., CALMELS D., CHADUTEAU C., CROS A., SAINT-BEZAR B., LANDREIN P. & DAVIS D. (2018) A big step in paleohydrological and diagenetic reconstructions in calcite veins and breccia of a sedimentary basin by combining Δ_{47} temperature, $\delta^{18}O_{water}$ and U-Pb age. *Chemical Geology*, 487, 1-17

PASSEY, B.H. & HENKES, G. A. (2012) Carbonate clumped isotope bond reordering and geospeedometry. *Earth Planet. Sci. Lett.,* 351–352, 223–236.

REGNET, J.B., ROBION, P., DAVID, C., FORTIN, J., BRIGAUD, B. & YVEN, B. (2014) Acoustic and reservoir properties of microporous carbonate rocks: implication of micrite particle size and morphology. *Journal of Geophysical Research: Solid Earth*, 120, 790 – 811.

RICHARD, J., SIZUN, J.-P., AND MACHHOUR L., 2007. Development and compartmentalization of chalky carbonate reservoirs : The Urgonian Jura-Bas Dauphiné platform model (Génissiat, southeastern France). Sedimentary Geology, 198, 195-207

ROBERSON H.E. & LAHANN R.W. (1981) - Smectite to illite conversion rates: effects of solution chemistry. Clays and Clay Minerals, 29, 129-135.

SAWATZKI, G.G., 1975. Etude géologique et minéralogique des flyschs du synclinal de Thônes (Haute-Savoie, France). Thèse 1643, Université de Genève. 148pp.

SCHAUBLE, E. A., GHOSH, P. & EILER, J.M. (2006) Preferential formation of $^{13}C–^{18}O$ bonds in carbonate minerals, estimated using first-principles lattice dynamics. *Geochim. Cosmochim. Acta*, 70, 2510–2529.

SCHEGG, R. (1992a) Coalification, shale diagenesis and thermal mod- elling in the Alpine foreland basin : The western Molasse Basin (Switzerland/France). *Organic Geochemistry*, 18, 289– 300.

SCHEGG, R. (1992b). Thermal maturity of the Swiss Molasse Basin: indications for paleogeothermal anomalies. *Eclogae Geol. Helv*., 85, 745–764.

SHENTON, B.J., GROSSMAN, E.L., PASSEY, B.H., HENKES, G. A., BECKER, T.P., LAYA, J.C., PEREZ-HUERTA, A., BECKER, S.P. & LAWSON, M. (2015) Clumped isotope thermometry in deeply buried sedimentary carbonates: The effects of bond reordering and recrystallization. *Geol. Soc. Am. Bull.*, n. B31169.1.

SCHIINFELD, J. (2000). Oxygen isotope composition of Upper Cretaceous chalk at Lägerdorf (NW Germany): its original environmental signal and palaeotemperature interpretation. Cretaceous Research, *1*2, 27–46.

SCHLAGER, W., & JAMES, N. P. (1978). Low-magnesian calcite limestones forming at the deep-sea floor, Tongue of the Ocean, Bahamas. *Sedimentology*, *25*, 675–702.

ŚRODON, J. (1980) Precise Identification of Illite/Smectite Interstratifications By X-Ray Powder Diffraction. *Clays Clay Miner*., 28, 401–411.

ŚRODOŃ J., & CLAUER N. (2001) Diagenetic history of Lower Palaeozoic sediments in Pomerania (northern Poland), traced across the Teisseyre-Tornquist tectonic zone using mixed-layer illite-smectite. *Clay minerals*, 36, 15-27.

ŚRODOŃ, J., CLAUER, N., HUFF, W., DUDEK, T. & BANAŚ, M. (2009) K-Ar dating of the Lower Palaeozoic K-bentonites from the Baltic Basin and the Baltic Shield: implications for the role of temperature and time in the illitization of smectite. *Clay minerals*, 44, 361-387.

STACHER, P. 1980. Stratigraphie, Mikrofazies und Mikropaläontologie der Wang Formation. Matér. Carte géol. Suisse, (n.s.) 152.

STOLPER, D.A. & EILER, J.M. (2016) Constraints on the formation and diagenesis of phosphorites using carbonate clumped isotopes. *Geochim. Cosmochim. Acta,* 181, 238–259.

ŠUCHA V., KRAUS I., GERTHOFFEROVÁ H., PETES J. & SEREKOVÁ M. (1993) Smectite to illite conversion in bentonites and shales of the East Slovak Basin. *Clay minerals,* 28, 243-253.

SWANSON, E.M., WERNICKE, B.P., EILER, J.M. & LOSH, S. (2012) Temperatures and fluids on faults based on carbonate clumped-isotope thermometry. *Am. J. Sci.*, 312, 1–21.

SWEENEY, J.J. & BURNHAM, A.K. (1990) Evaluation of a simple model of vitrinite reflectance based on chemical kinetics. *Am. Assoc. Pet. Geol. Bull*., 74, 1559–1570.

THYBERG B., JAHREN J., WINJE T., BJØRLYKKE K., FALEIDE J.I. & MARCUSSEN Ø. (2010) Quartz cementation in Late Cretaceous mudstones, northern North Sea: Changes in rock properties due to dissolution of smectite and precipitation of micro-quartz crystals. *Marine and Petroleum Geology*, 27, 1752–1764

VILLARD, F. (1988) Progradation de la Formation de Wang dans les chaînes subalpines septentrionales (Alpes occidentales, France) au Maastrichtien supérieur : biostratigraphie et milieu de dépôt. *Eclogae geol. Helv*. 81, 3, 669-687

VILLARD F., 1991. Evolution paléogéographique du domaine delphino-helvétique (entre Chartreuse et Morcles) au Crétacé supérieur (Turonien-Maastrichtien): Biostratigraphie, sédimentologie et dynamique sédimentaire sur une rampe carbonatée. Pub. Département Géologie-Paléontologie, Université de Genève, n° 10, 173 p.

WATKINS, J. M., NIELSEN, L. C., RYERSON, F. J., & DEPAOLO, D. J. (2013). The influence of kinetics on the oxygen isotope composition of calcium carbonate. *Earth and Planetary Science Letters*, *375*, 349–360.

WINKELSTERN, I.Z. & LOHMANN, K.C.(2016) Shallow burial alteration of dolomite and limestone clumped isotope geochemistry. *Geology*, 44, 467–470.

ZINSNER, B. & F. M. PELLERIN. (2007) A geoscientist's guide to petrophysics: Paris, France, *Editions Technip*, 450 pp.

FIGURES CAPTIONS

Figure 1. Geological context of the studied area. A. Simplified structural sketch map of the northern subalpine chains (Bornes and Bauges massifs, France, showing the main thrust units. B. Detailed elevation map of the area. The different numbers (1 to 18) refer to the location of the studied sections, whereas the colors refer to the geographic and tectonic domains they belong to: outer A domain (yellow), intermediate B domain (orange) and inner C domain (red). C. Simplified stratigraphic succession (Late Jurassic-Paleogene) of the northern subalpine massifs, with location of the stratigraphic intervals targeted for paleothermal reconstruction. Black star: "sublithographic limestones" investigated for clay mineral diagenesis and Δ_{47} thermometry. Red star: Wang formation used to measure organic matter maturity by Gorin & Monteil, (1990).

Figure 2. Relative proportions of clay minerals in each investigated samples collected from eighteen sites falling in three structural domains (A, B, C), with respect to their illite content in I-S mixed layers. From top to base, are illustrated the results for samples (numbers 1 to 18) located from the external A domain toward the internal C domain of the Bauges and Bornes

massifs. The estimations of illite content in I-S mixed layers are highlighted with black dots when using the methods of Środoń (1980; 1984) and with red dots when using the method of Inoue et al. (1989). Note how samples from a single stratigraphic interval, within in a small geographic area, can be significantly differentiated based on their clay mineral assemblages and illite content in the I-S mixed layers.

Figure 3. Example of X-ray diffraction pattern of I-S (002/003) peak, for the <2µm fraction after glycolation. The results for six representative samples, belonging to the A, B and C domains, are shown.

Table 1. Summary of mineralogical, petrophysical and geochemical data available for the studied area

Figure 4. Petrographic and petrophysical properties of the investigated samples. A. Macrophotography of the Upper Cretaceous sublithographic limestones outcropping in the studied area. B. Scanning electron microscopy (SEM) microphotographs used to characterize micrite microtextures and quantify crystallometry parameter of the investigated samples. Picture are taken at the magnification x10000. C. Histograms illustrating the variability of the crystallometry parameter measured for the micrite samples, defined by the maximum 2D length of particles measured on SEM photomicrographs at x5000 magnification. Note that all the investigated samples, belonging to the A, B and C domains, do not display any significant difference in term of microtextures (particles shapes, contact between grains, crystallometry) and petrophysical properties (porosity and permeability).

Figure 5. Micrite stable isotope data. **A.** Cross-plot $\delta^{18}O_{carb}$ versus $\delta^{13}C_{carb}$ composition of micrite samples from the A, B and C domains. Uncertainties are smaller than the dot size. $\delta^{18}O_{carb}$ and $\delta^{13}C_{carb}$ values from unaltered Upper Cretaceous marine shells (Veizer et al. 1999) are illustrated with grey boxes, whereas those of deep-chalk deposits suffering some amount of alteration are highlighted with a black box (Jenkyns et al. 1994 and Schiinfeld et al. 1991). **B**. Cross-plot of $\delta^{18}O_{carb}$ versus the temperatures calculated from Δ_{47} in the micrite samples from the A, B and C domains. Circled 1 and 2 and associated black arrows refer to trends resulting from recrystallization of calcite at temperatures higher than depositional ones (1) and Δ_{47} thermal resetting (2). The grey box represents $\delta^{18}O_{carb}$ composition of unaltered Upper Cretaceous marine shells (Veizer et al. 1999), combined with coeval shallow seawater temperature from Jenkyns et al. 1994 (ie. between 20 and 26°C). Reported uncertainties on data are 1 S.D. of the replicate analyses for $T\Delta_{47}$, and are smaller than the dot size for $\delta^{18}O$. **C.** 3D diagram showing the relationship between $\delta^{13}C_{carb}$, $\delta^{18}O_{carb}$ and $T\Delta_{47}$ measured in the investigated samples. The solid arrow illustrates the observed trend of Δ_{47} thermal resetting from the A and B domains toward the C domain. Uncertainties are not represented in the 3D diagram.

Figure 6. Summary of the paleothermometric data available for the Upper Cretaceous series of the studied area. A general correlation has been recognized between the amount of illite layers in I-S (panel B), vitrinite maturity (panel C), Rock-Eval T_{max} (panel D) and Δ_{47} temperatures (panel E). Samples from the most internal C domain display illite content in I-S mixed layer systematically higher than 90%, vitrinite reflectance Ro% values up to 1.3% and Δ_{47} temperatures higher than 150°C. In contrast, samples from the most external A domain record % illite in I-S between 20 and 50% (I-S R0), lower vitrinite maturity (Ro% = 0.45-

0.55) and cooler Δ_{47} temperatures of ~40-60°C. Such results point out a clear increase of thermal maturity of samples from the A domain toward the C domain and demonstrate that samples collected within a restricted geographic area may record very different thermal maturities.

Figure 7. Thermal modeling of paleothermometric data using seven conceptual time-temperature scenarios (Th1 to Th7) and the respective kinetic algorithms relevant to the employed paleothermometers (c.f. Sweeney and Burnham, 1990 for Ro% model; Henkes et al. (2013) for Δ_{47} C-O bond reordering and Huang et al., 1993 for smectite to illite conversion in I-S). The model predictions are here compared to the measured values in samples A1, B9 and C16 from which paired TΔ_{47}, Ro% and I% data were available. In B, C and D is shown the evolution of Δ_{47} temperatures, Ro% values, and % illite in I-S mixed layer over time computed using the different input thermal histories (i.e. maximal burial temperature from 80°C for TH1 in blue, up to 180°C for TH7 in red). The two prograde thermal histories proposed by Burrus, (1991) (TH1 in blue and TH6 in orange) are noted here with an asterisk, whereas all the others mid-scenarios were conceptually defined. The black rectangles on the right side of the diagrams represent the measured values for each paleothermometric proxy.

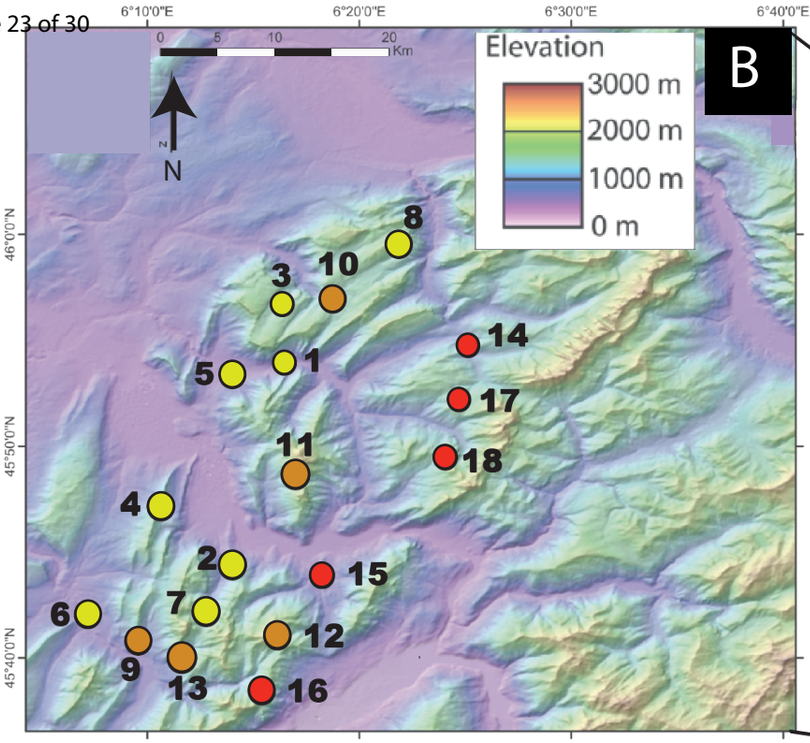

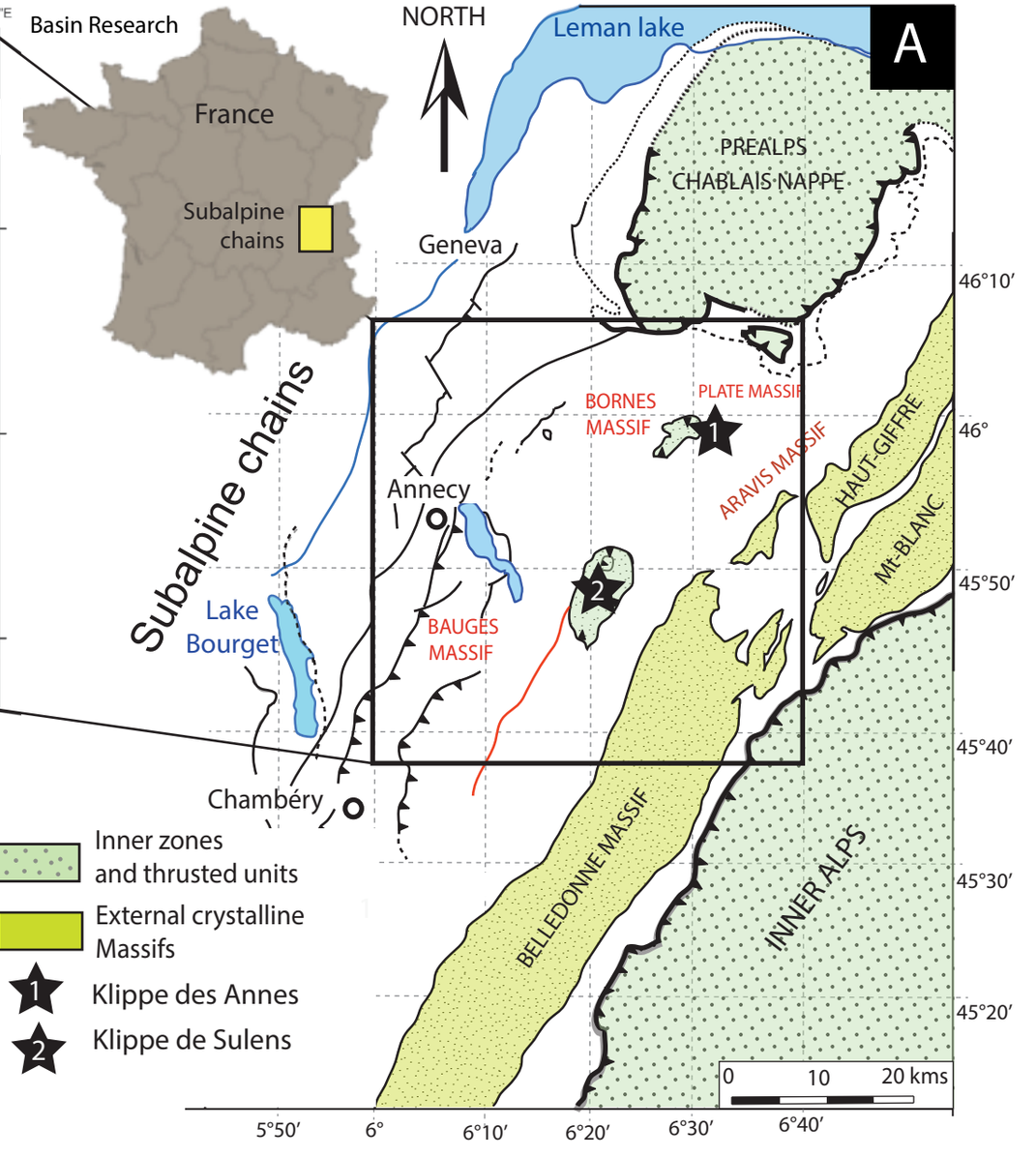

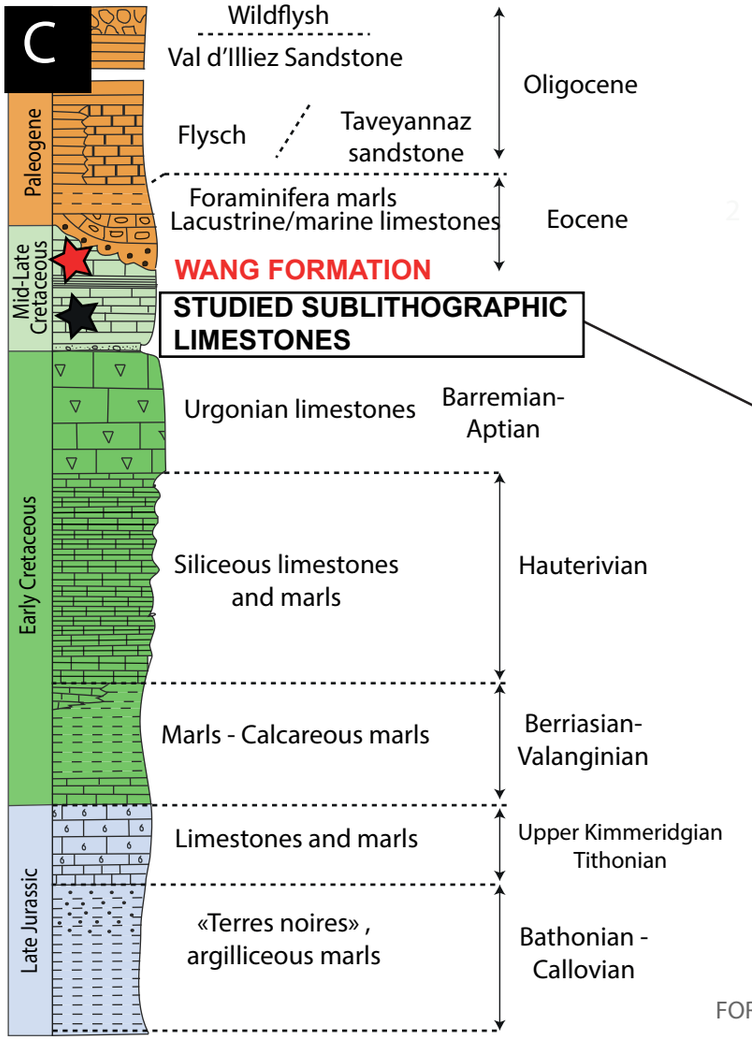

Domain A

1. Crêt des Tervelles
2. La Motte-en-Bauges
3. Lindion
4. Avellard
5. Les Garins
6. Chatelard
7. Trélod
8. Synclinal de Thônes

Domain B

9. Grand Colombier
10. Les Auges
11. Arclozan
12. Bellevaux
13. Ecole en Bauges

Domain C

14. La Clusaz
15. Seythenex
16. Nant de la Chapelle
17. La Blonniere
18. Cul d'Ugine

Stratigraphic interval invesigated for :

Organic matter maturity (Gorin and Monteuil, 1990)

Clay minerals and Δ_{47} thermometry (this study)

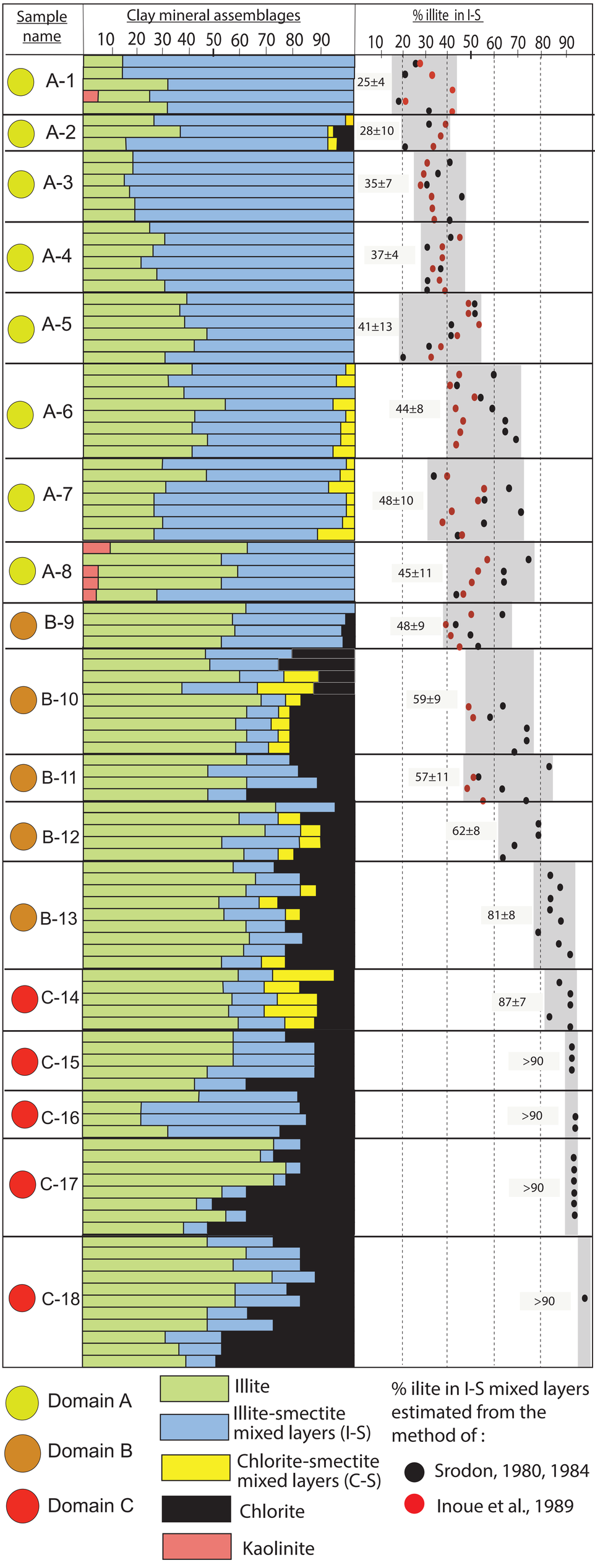
Sample name
Clay mineral assemblages
10 20 30 40 50 60 70 80 90
% illite in I-S
10 20 30 40 50 60 70 80 90
A-1
25±4
A-2
28±10
A-3
35±7
A-4
37±4
A-5
41±13
A-6
44±8
A-7
48±10
A-8
45±11
B-9
48±9
B-10
59±9
B-11
57±11
B-12
62±8
B-13
81±8
C-14
87±7
C-15
>90
C-16
>90
C-17
>90
C-18
>90
Domain A
Domain B
Domain C
Illite
Illite-smectite mixed layers (I-S)
Chlorite-smectite mixed layers (C-S)
Chlorite
Kaolinite
% ilite in I-S mixed layers estimated from the method of :
Srodon, 1980, 1984
Inoue et al., 1989

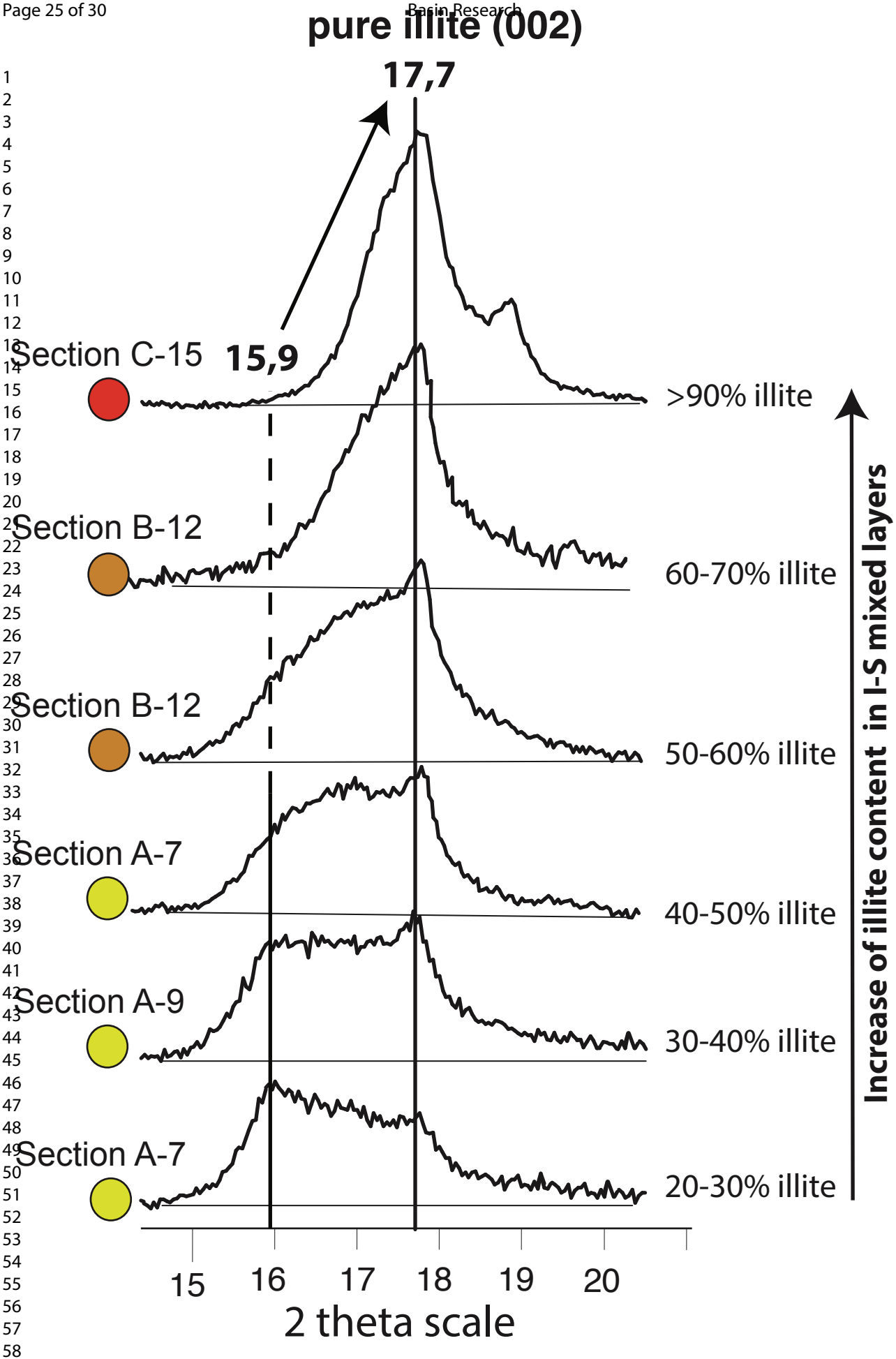
pure illite (002)
17,7
15,9
Section C-15
>90% illite
Section B-12
60-70% illite
Section B-12
50-60% illite
Section A-7
40-50% illite
Section A-9
30-40% illite
Section A-7
20-30% illite
Increase of illite content in I-S mixed layers
15
16
17
18
19
20
2 theta scale

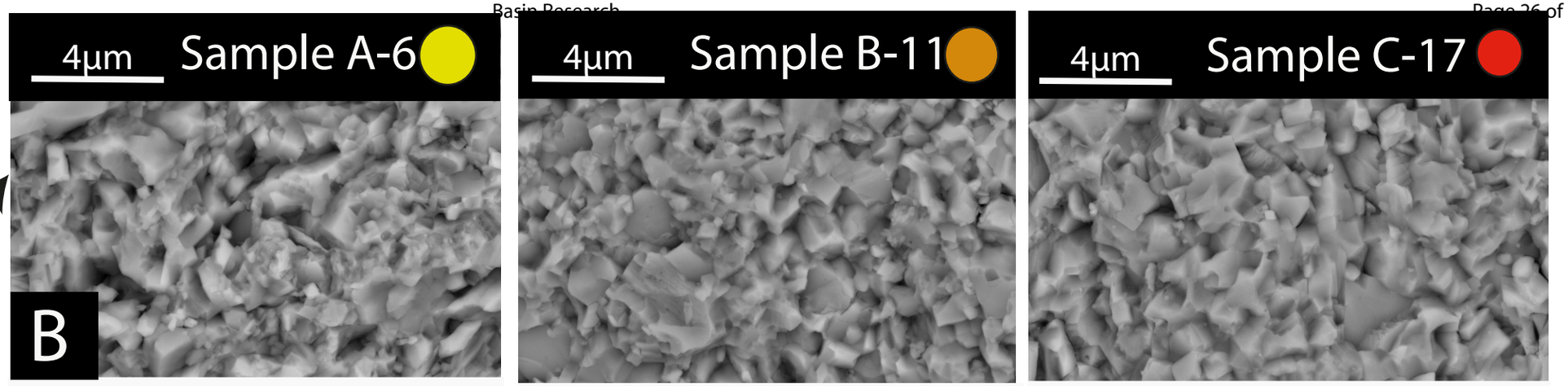

Particle shape : Anhedral-subhedral compact
Contact : Coalescent
Crystallometry : 1.31µm
Ø : 1,07%., K <0.001MDa

Particle shape : Anhedral-subhedral compact
Contact : Coalescent
Crystallometry : 1.43µm
Ø : 0.51% ; K <0.001MDa

Particle shape : Anhedral-subhedral compact
Contact : Coalescent
Crystallometry : 1,45µm
Ø : 0.56% ; K <0.001MDa

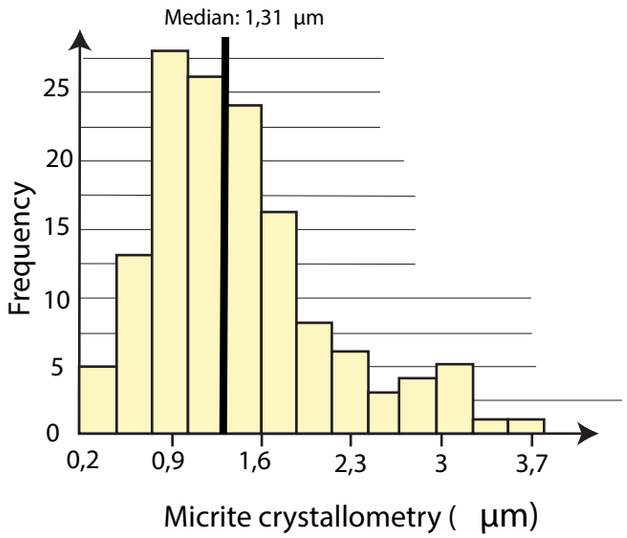

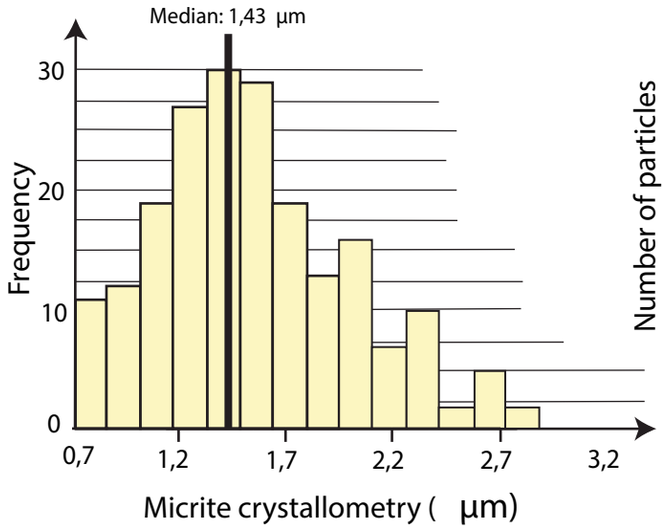

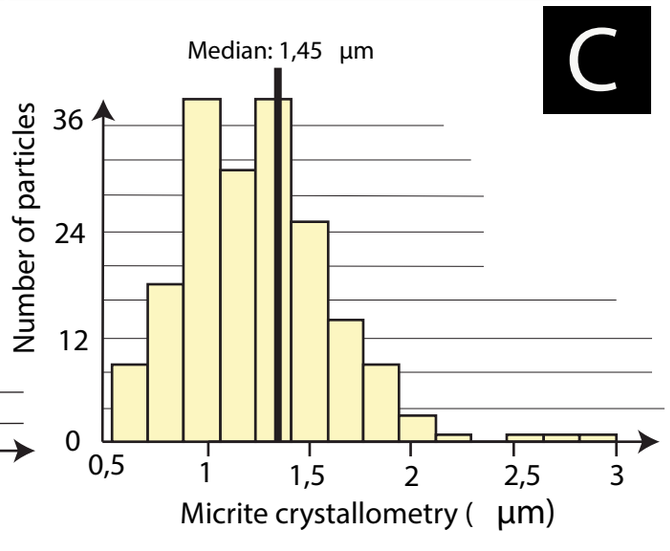

		Clay fraction (<5%)			Carbonated fraction (>95%)								Organic matter-bearing Wang Formation [6]	
		Illite content in I-S [1]			Micrite particles [2]		Petrophysical		Stable isotope data					
		Min	Max	Reichweite Nb.	Text.	Crystallo.	Φ	K	$\delta^{18}O$	$\delta^{13}C$	$\Delta47$ [3]	$T\Delta_{47}$ [4]	$\delta^{18}O_{water}$ [5]	Ro%	Tmax
	Sample	%	%	-	-	um	%	mD	‰ (VPDB)	‰ (VPDB)	(CDES25)	°C	‰ (SMOW)	%	(°C)
DOMAIN A	A1	18	42	R0	Anhed.Comp.	1,43 (141)	0.522	<0.001	-3.48±0.05	0.04±0.01	0.597±0.032 (4)	**61±14**	3.6	0.45±0.05	428
	A2	21	40	R0	-	-	-	-	-	-	-	-	-	-	-
	A3	28	42	R0	-	-	-	-	-	-	-	-	-	-	-
	A4	30	45	R0	-	-	-	-	-	-	-	-	-	-	-
	A5	20	50	R0	-	-	-	-	-	-	-	-	-	-	-
	A6	40	65	R0/R1	Anhed.Comp.	1,31 (189)	1.073	0.001	-3.89±0.05	1.69±0.01	0.633±0.010 (2)	**46±7**	0.7	0.55±0.05	430
	A7	35	65	R0/R1	-	-	-	-	-	-	-	-	-	-	-
	A8	40	70	R0/R1	-	-	-	-	-	-	-	-	-	-	-
DOMAIN B	B9	40	65	R0/R1	-	-	1.36	0.008	-3.54±0.04	2.01±0.07	0.613±0.022 (3)	**54±9**	2.4	0.7±0.1	437
	B10	50	78	R1	-	-			-	-	-	-	-	-	-
	B11	50	82	R1	Anhed.Comp.	1,43 (132)	0.508	<0.001	-	-	-	-	-	-	-
	B12	60	80	R1	-	-	0.555	<0.001	-3.53±0.21	2.39±0.07	0.634±0.076 (2)	**45±30**	0.8	-	-
	B13	78	90	R1	-	-	-	-	-	-	-	-	-	-	-
Average for domain A and B									**-3.61±0.19‰**	**1.53±1 ‰**	**0.619±0.017**	**51±7°C**	**1.7±1.3**		
DOMAIN C	C14	80	90	R1/R3	-	-	-	-	-	-	-	-	-	-	-
	C15	90	100	R3	Anhed.Comp.	1,78 (146)	0.984	<0.001	-3.27±0.05	2.42±0.05	0.429±0.049 (2)	**174±54**	17.3	-	-
	C16	90	100	R3	-	-	-	-	-3.15±0.06	2.02±0.06	0.434±0.018 (3)	**169±19**	17	1.3±0.2	461-474
	C17	90	100	R3	Anhed.Comp.	1,45 (205)	0.559	<0.001	-3.57±0.15	2.90±0.06	0.400±0.041 (2)	**208±56**	19.9		-
	C18	90	100	R3	-	-	-	-	-3.66±0.09	2.55±0.03	0.423±0.039 (4)	**181±44**	17.5	-	-
Average for domain C									**-3.41±0.24‰**	**2.47±0.4 ‰**	**0.421±0.015**	**183±17°C**	**17.9±1.3**		

(1) Illite content in I-S mixed layers were estimated following the methods of Srodon, 1984 and Inoue et et al. 1989. R0 = illite <50% ; R1 = illite between 50 and 90% ; R3 : illite >90%

(2) Micrite particles texture (text.) and crystallography parameter (Crystallo.) were characterized by SEM images point couting. The number of crystallography values measured for each section is notify in brackets.

(3) Δ_{47} values relative to the CDES (or 'carbon dioxide equilibrium scale') and the 25°C acid digestion frames (an acid correction factor of 0.092‰ was applied following Henkes et al. 2013). D47 values are reported with their respective one standard deviation of the mean (1 S.D.) for replicate measurements of the same powder. In brackets is the number of replicate measurements of the same carbonate powder. (4) Paleotemperatures calculated using the universal Δ47-temperature calibration from Bonifacie et al. 2017. Reported uncertainties are calculated based on the S.D. reported for Δ_{47} values.

(5) Oxygen isotope compositions of the fluid in equilibrium with the carbonate calculated using T Δ_{47} and the fractionation factor of oxygen isotopes between calcite and water of Watkins et al. (2013). (6) Vitrinite reflectance and Tmax values were measured by Gorin and Monteuil, 1990 in the overlying Cretaceous Wang Formation, and in the same or very close localities.

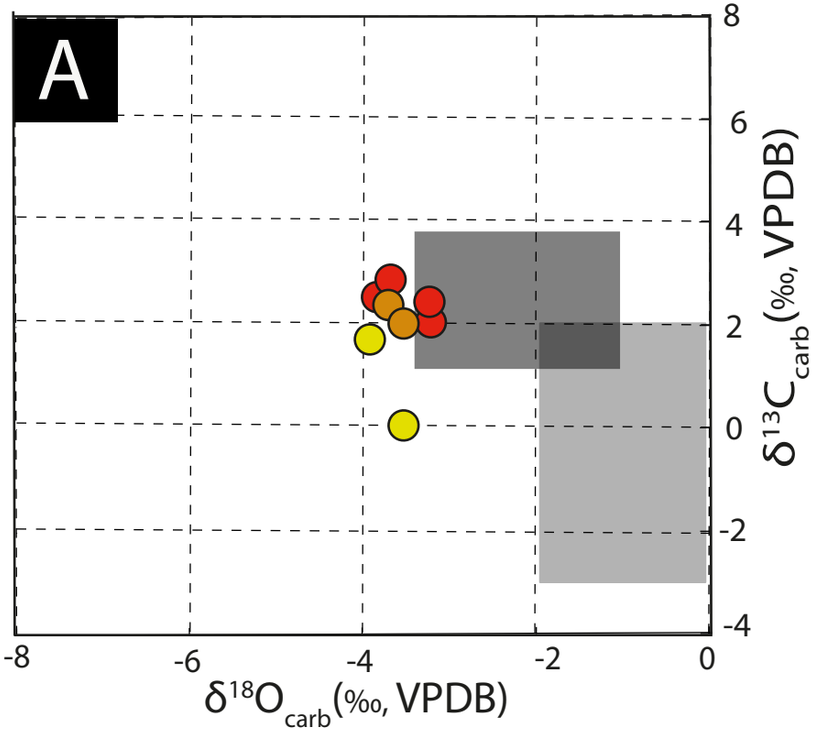

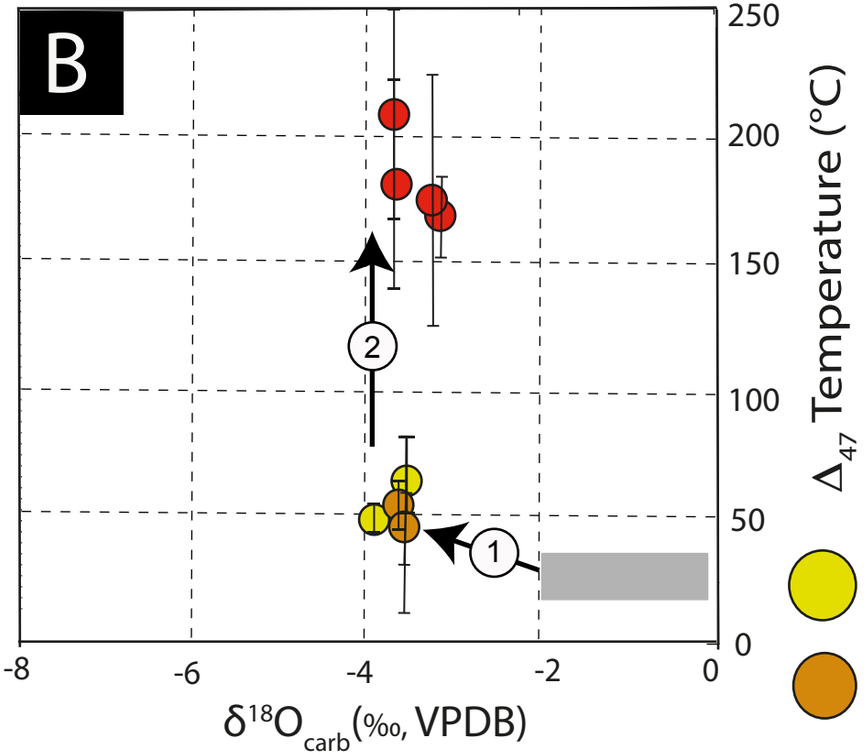

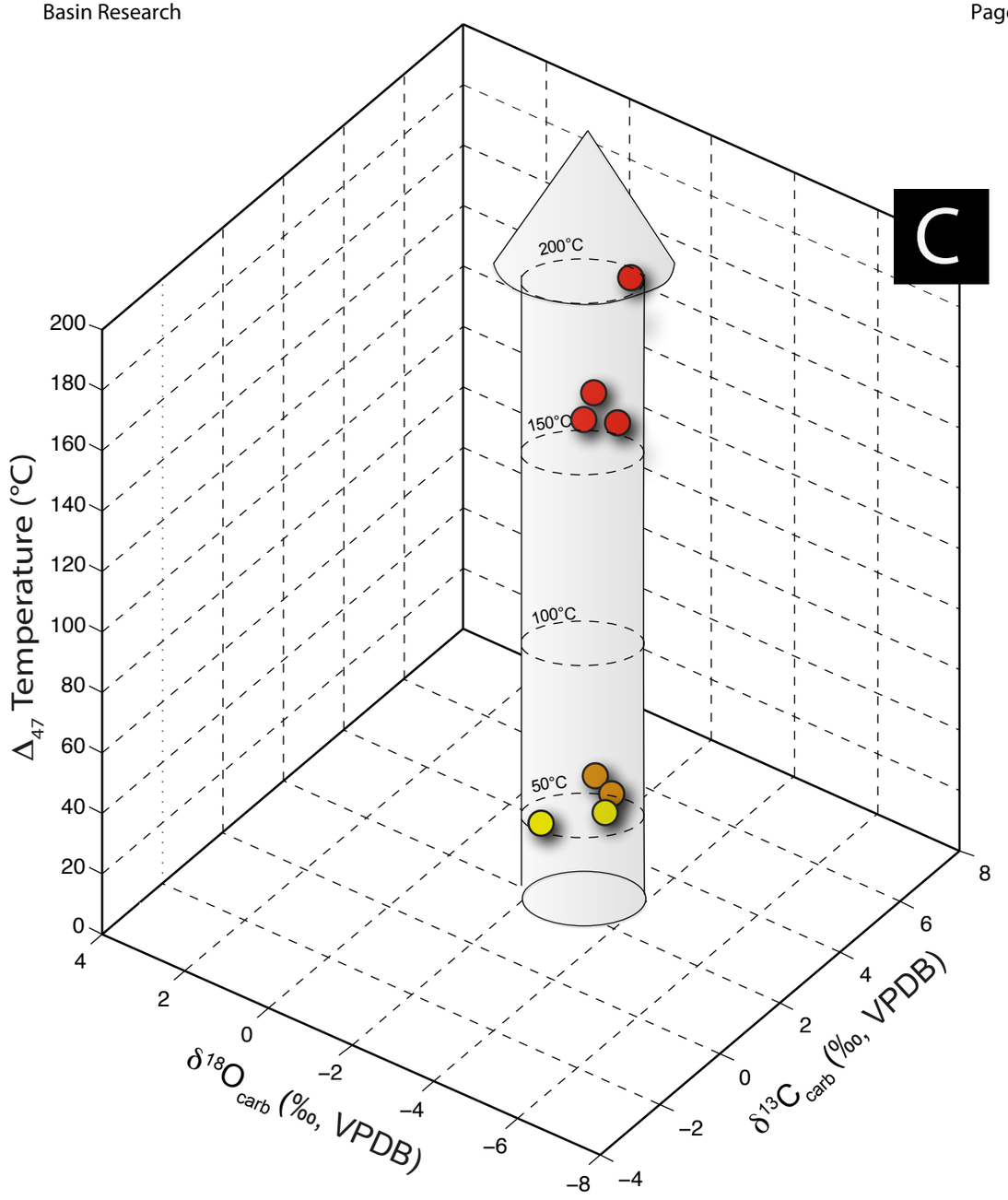

Domain A
samples A1, A6

Domain B
samples B9, B12

Domain C
samples C15, C16, C17, C18

Upper Cretaceous Low Magnesium Calcite shells
Veizer et al. (1999)

Upper Cretaceous chalk with diagenetic alteration
Jenkyns et al. (1994)
Schiinfeld et al. (1991)

1 Recrystallization at ±50°C and $\delta^{18}O_{water}$ of 1.7±1.2‰

2 Δ_{47} thermal resseting

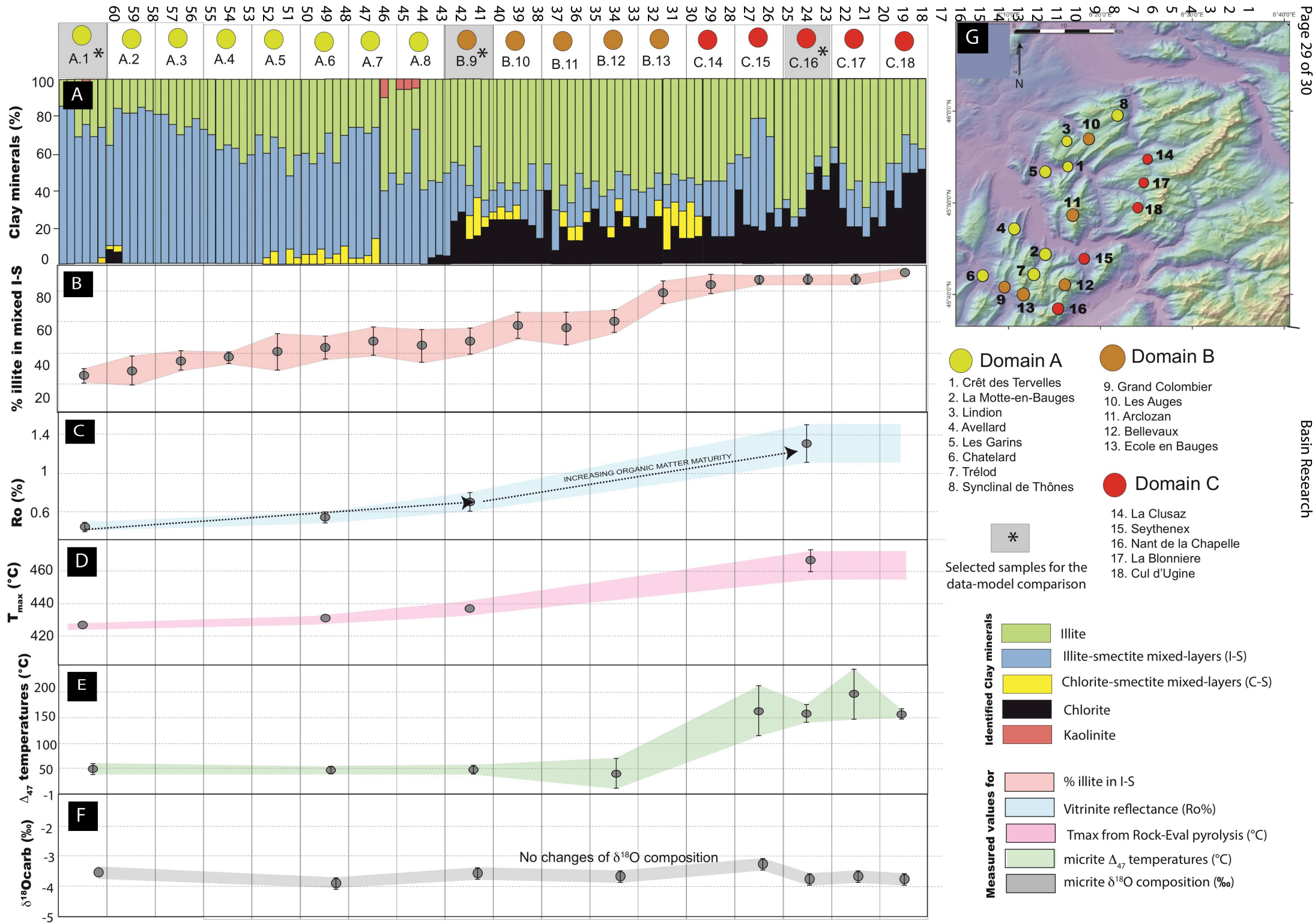
A.1 *
A.2
A.3
A.4
A.5
A.6
A.7
A.8
B.9 *
B.10
B.11
B.12
B.13
C.14
C.15
C.16 *
C.17
C.18
A
Clay minerals (%)
B
% illite in mixed I-S
C
Ro (%)
INCREASING ORGANIC MATTER MATURITY
D
T_{max} (°C)
E
Δ_{47} temperatures (°C)
F
δ^{18}Ocarb (‰)
No changes of δ^{18}O composition
G
N
Domain A
1. Crêt des Tervelles
2. La Motte-en-Bauges
3. Lindion
4. Avellard
5. Les Garins
6. Chatelard
7. Trélod
8. Synclinal de Thônes
Domain B
9. Grand Colombier
10. Les Auges
11. Arclozan
12. Bellevaux
13. Ecole en Bauges
Domain C
14. La Clusaz
15. Seythenex
16. Nant de la Chapelle
17. La Blonniere
18. Cul d'Ugine
* Selected samples for the data-model comparison
Identified Clay minerals
Illite
Illite-smectite mixed-layers (I-S)
Chlorite-smectite mixed-layers (C-S)
Chlorite
Kaolinite
Measured values for
% illite in I-S
Vitrinite reflectance (Ro%)
Tmax from Rock-Eval pyrolysis (°C)
micrite Δ_{47} temperatures (°C)
micrite δ^{18}O composition (‰)